Modeling the Influence of Irradiation Temperature and Displacement Rate on Radiation-Induced Hardening in Ferritic Steels

Prepared by
R. E. Stoller

Oak Ridge National Laboratory

Modeling the Influence of Irradiation Temperature and Displacement Rate on Radiation-Induced Hardening in Ferritic Steels

Prepared by
R. E. Stoller

Oak Ridge National Laboratory
Managed by Martin Marietta Energy Systems, Inc.

Oak Ridge National Laboratory
Oak Ridge, TN 37831-6285

Abstract

The influence of irradiation temperature and displacement rate have been investigated using a model based on the reaction rate theory description of radiation damage. This theory was developed primarily for the investigation of relatively high-temperature, high-dose radiation effects such as void swelling and irradiation creep. Before applying that theory to the much lower temperature and dose regimes characteristic of light water reactor pressure vessels and support structures, it is necessary to examine the assumptions made in formulating the theory. The major simplifying assumption that has commonly been made is that the interstitial and vacancy concentrations reach a quasi-steady state condition rapidly enough that the steady state concentrations can be used in calculating the observable radiation effects. The results presented here indicate that the assumption of steady state point defect concentrations is not valid for temperatures much below the light water reactor pressure vessel operating temperature of about 288°C. At lower temperatures, the time required for the point defect concentrations to reach steady state can exceed an operating reactor's lifetime. Even at 288°C, the point defect transient time can be long enough to influence the interpretation of irradiation experiments done in materials test reactors at accelerated damage rates.

Based on the insights obtained with the simple models of point defect evolution, a more detailed model was developed that incorporates an explicit description of point defect clustering. These clusters are potentially responsible for the fraction of the radiation-induced hardening that is attributed to the so-called "matrix defect." The model considers both interstitial and vacancy clustering. The former are treated as Frank loops while the later are treated as microvoids. The point defect clusters can be formed either directly in the displacement cascade or by diffusive encounters between free point defects. The results of molecular dynamics simulation studies are used to provide guidance for the clustering parameters. The hardening due to point defect clusters was calculated using a simple dislocation barrier model. The results indicate that both interstitial and vacancy clusters can give rise to significant hardening. The relative importance of each cluster type is shown to be a function of irradiation temperature and displacement rate.

Contents

Figures

Tables

Foreword

The work reported here was performed at the Oak Ridge National Laboratory (ORNL) under the Heavy-Section Steel Irradiation (HSSI) Program, W. R. Corwin, Program Manager. The program is sponsored by the Office of Nuclear Regulatory Research of the U.S. Nuclear Regulatory Commission (NRC). The technical monitor for the NRC is E. M. Hackett.

This report is designated HSSI Report 5. Reports in this series are listed below:

1. F. M. Haggag, W. R. Corwin, and R. K. Nanstad, Martin Marietta Energy Systems, Inc., Oak Ridge Natl. Lab., Oak Ridge, Tenn., *Irradiation Effects on Strength and Toughness of Three-Wire Series-Arc Stainless Steel Weld Overlay Cladding*, NUREG/CR-5511 (ORNL/TM-11439), February 1990.

2. L. F. Miller, C. A. Baldwin, F. W. Stallman, and F. B. K. Kam, Martin Marietta Energy Systems, Inc., Oak Ridge Natl. Lab., Oak Ridge, Tenn., *Neutron Exposure Parameters for the Metallurgical Test Specimens in the Sixth Heavy-Section Steel Irradiation Series*, NUREG/CR-5409 (ORNL/TM-11267), March 1990.

3. S. K. Iskander, W. R. Corwin, and R. K. Nanstad, Martin Marietta Energy Systems, Inc., Oak Ridge Natl. Lab., Oak Ridge, Tenn., *Results of Crack-Arrest Tests on Two Irradiated High-Copper Welds*, NUREG/CR-5584 (ORNL/TM-11575), December 1990.

4. R. K. Nanstad and R. G. Berggren, Martin Marietta Energy Systems, Inc., Oak Ridge Natl. Lab., Oak Ridge, Tenn., *Irradiation Effects on Charpy Impact and Tensile Properties of Low Upper-Shelf Welds, HSSI Series 2 and 3*, NUREG/CR-5696 (ORNL/TM-11804), August 1991.

5. This report.

The HSSI Program includes both follow-on and the direct continuation of work that was performed under the Heavy-Section Steel Technology (HSST) Program. Previous HSST reports related to irradiation effects in pressure vessel materials and those containing unirradiated properties of materials used in HSSI and HSST irradiation programs are tabulated below as a convenience to the reader.

C. E. Childress, Union Carbide Corp. Nuclear Div., Oak Ridge Natl. Lab., Oak Ridge, Tenn., *Fabrication History of the First Two 12-in.-Thick A-533 Grade B, Class 1 Steel Plates of the Heavy Section Steel Technology Program*, ORNL-4313, February 1969.

T. R. Mager and F. O. Thomas, Westinghouse Electric Corporation, PWR Systems Division, Pittsburgh, Pa., *Evaluation by Linear Elastic Fracture Mechanics of Radiation Damage to Pressure Vessel Steels*, WCAP-7328 (Rev.), October 1969.

P. N. Randall, TRW Systems Group, Redondo Beach, Calif., *Gross Strain Measure of Fracture Toughness of Steels*, HSSTP-TR-3, Nov. 1, 1969.

L. W. Loechel, Martin Marietta Corporation, Denver, Colo., *The Effect of Testing Variables on the Transition Temperature in Steel*, MCR-69-189, November 20, 1969.

W. O. Shabbits, W. H. Pryle, and E. T. Wessel, Westinghouse Electric Corporation, PWR Systems Division, Pittsburgh, Pa., *Heavy-Section Fracture Toughness Properties of A533 Grade B Class 1 Steel Plate and Submerged Arc Weldment*, WCAP-7414, December 1969.

C. E. Childress, Union Carbide Corp. Nuclear Div., Oak Ridge Natl. Lab., Oak Ridge, Tenn., *Fabrication History of the Third and Fourth ASTM A-533 Steel Plates of the Heavy Section Steel Technology Program*, ORNL-4313-2, February 1970.

P. B. Crosley and E. J. Ripling, Materials Research Laboratory, Inc., Glenwood, Ill., *Crack Arrest Fracture Toughness of A533 Grade B Class 1 Pressure Vessel Steel*, HSSTP-TR-8, March 1970.

F. J. Loss, Naval Research Laboratory, Washington, D.C., *Dynamic Tear Test Investigations of the Fracture Toughness of Thick-Section Steel*, NRL-7056, May 14, 1970.

T. R. Mager, Westinghouse Electric Corporation, PWR Systems Division, Pittsburgh, Pa., *Post-Irradiation Testing of 2T Compact Tension Specimens*, WCAP-7561, August 1970.

F. J. Witt and R. G. Berggren, Union Carbide Corp. Nuclear Div., Oak Ridge Natl. Lab., Oak Ridge, Tenn., *Size Effects and Energy Disposition in Impact Specimen Testing of ASTM A533 Grade B Steel*, ORNL/TM-3030, August 1970.

D. A. Canonico, Union Carbide Corp. Nuclear Div., Oak Ridge Natl. Lab., Oak Ridge, Tenn., *Transition Temperature Considerations for Thick-Wall Nuclear Pressure Vessels*, ORNL/TM-3114, October 1970.

T. R. Mager, Westinghouse Electric Corporation, PWR Systems Division, Pittsburgh, Pa., *Fracture Toughness Characterization Study of A533, Grade B, Class 1 Steel*, WCAP-7578, October 1970.

W. O. Shabbits, Westinghouse Electric Corporation, PWR Systems Division, Pittsburgh, Pa., *Dynamic Fracture Toughness Properties of Heavy Section A533 Grade B Class 1 Steel Plate*, WCAP-7623, December 1970.

C. E. Childress, Union Carbide Corp. Nuclear Div., Oak Ridge Natl. Lab., Oak Ridge, Tenn., *Fabrication Procedures and Acceptance Data for ASTM A-533 Welds and a 10-in.-Thick ASTM A-543 Plate of the Heavy Section Steel Technology Program*, ORNL-TM-4313-3, January 1971.

D. A. Canonico and R. G. Berggren, Union Carbide Corp. Nuclear Div., Oak Ridge Natl. Lab., Oak Ridge, Tenn., *Tensile and Impact Properties of Thick-Section Plate and Weldments*, ORNL/TM-3211, January 1971.

C. W. Hunter and J. A. Williams, Hanford Eng. Dev. Lab., Richland, Wash., *Fracture and Tensile Behavior of Neutron-Irradiated A533-B Pressure Vessel Steel*, HEDL-TME-71-76, February 6, 1971.

C. E. Childress, Union Carbide Corp. Nuclear Div., Oak Ridge Natl. Lab., Oak Ridge, Tenn., *Manual for ASTM A533 Grade B Class 1 Steel (HSST Plate 03) Provided to the International Atomic Energy Agency*, ORNL/TM-3193, March 1971.

P. N. Randall, TRW Systems Group, Redondo Beach, Calif., *Gross Strain Crack Tolerance of A533-B Steel*, HSSTP-TR-14, May 1, 1971.

C. L. Segaser, Union Carbide Corp. Nuclear Div., Oak Ridge Natl. Lab., Oak Ridge, Tenn., *Feasibility Study, Irradiation of Heavy-Section Steel Specimens in the South Test Facility of the Oak Ridge Research Reactor*, ORNL/TM-3234, May 1971.

H. T. Corten and R. H. Sailors, University of Illinois, Urbana, Ill., *Relationship Between Material Fracture Toughness Using Fracture Mechanics and Transition Temperature Tests*, T&AM Report 346, August 1, 1971.

L. A. James and J. A. Williams, Hanford Eng. Dev. Lab., Richland, Wash., *Heavy Section Steel Technology Program Technical Report No. 21, The Effect of Temperature and Neutron Irradiation Upon the Fatigue-Crack Propagation Behavior of ASTM A533 Grade B, Cl. Steel*, HEDL-TME 72-132, September 1972.

P. B. Crosley and E. J. Ripling, Materials Research Laboratory, Inc., Glenwood, Ill., *Crack Arrest in an Increasing K-Field*, HSSTP-TR-27, January 1973.

W. J. Stelzman and R. G. Berggren, Union Carbide Corp. Nuclear Div., Oak Ridge Natl. Lab., Oak Ridge, Tenn., *Radiation Strengthening and Embrittlement in Heavy-Section Steel Plates and Welds*, ORNL-4871, June 1973.

J. M. Steichen and J. A. Williams, Hanford Eng. Dev. Lab., Richland, Wash., *High Strain Rate Tensile Properties of Irradiated ASTM A533 Grade B Class 1 Pressure Vessel Steel*, HEDL-TME 73-74, July 1973.

J. A. Williams, Hanford Eng. Dev. Lab., Richland, Wash., *The Irradiation and Temperature Dependence of Tensile and Fracture Properties of ASTM A533, Grade B, Class 1 Steel Plate and Weldment*, HEDL-TME 73-75, August 1973.

J. A. Williams, Hanford Eng. Dev. Lab., Richland, Wash., *Some Comments Related to the Effect of Rate on the Fracture Toughness of Irradiated ASTM A553-B Steel Based on Yield Strength Behavior*, HEDL-SA 797, December 1974.

J. A. Williams, Hanford Eng. Dev. Lab., Richland, Wash., *The Irradiated Fracture Toughness of ASTM A533, Grade B, Class 1 Steel Measured with a Four-Inch-Thick Compact Tension Specimen*, HEDL-TME 75-10, January 1975.

J. G. Merkle, G. D. Whitman, and R. H. Bryan, Union Carbide Corp. Nuclear Div., Oak Ridge

Natl. Lab., Oak Ridge, Tenn., *An Evaluation of the HSST Program Intermediate Pressure Vessel Tests in Terms of Light-Water-Reactor Pressure Vessel Safety*, ORNL/TM-5090, November 1975.

J. A. Davidson, L. J. Ceschini, R. P. Shogan, and G. V. Rao, Westinghouse Electric Corporation, Pittsburgh, Pa., *The Irradiated Dynamic Fracture Toughness of ASTM A533, Grade B, Class 1 Steel Plate and Submerged Arc Weldment*, WCAP-8775, October 1976.

J. A. Williams, Hanford Eng. Dev. Lab., Richland, Wash., *Tensile Properties of Irradiated and Unirradiated Welds of A533 Steel Plate and A508 Forgings*, NUREG/CR-1158 (ORNL/SUB-79/50917/2), July 1979.

J. A. Williams, Hanford Eng. Dev. Lab., Richland, Wash., *The Ductile Fracture Toughness of Heavy Section Steel Plate*, NUREG/CR-0859, September 1979.

K. W. Carlson and J. A. Williams, Hanford Eng. Dev. Lab., Richland, Wash., *The Effect of Crack Length and Side Grooves on the Ductile Fracture Toughness Properties of ASTM A533 Steel*, NUREG/CR-1171 (ORNL/SUB-79/50917/3), October 1979.

G. A. Clarke, Westinghouse Electric Corp., Pittsburgh, Pa., *An Evaluation of the Unloading Compliance Procedure for J-Integral Testing in the Hot Cell, Final Report*. NUREG/CR-1070 (ORNL/Sub-7244/1), October 1979.

P. B. Crosley and E. J. Ripling, Materials Research Laboratory, Inc., Glenwood, Ill., *Development of a Standard Test for Measuring K_{Ia} with a Modified Compact Specimen*, NUREG/CR-2294 (ORNL/SUB-81/7755/1), August 1981.

H. A. Domian, Babcock and Wilcox Company, Alliance, Ohio, *Vessel V-8 Repair and Preparation of Low Upper-Shelf Weldment*, NUREG/CR-2676 (ORNL/Sub/81-85813/1), June 1982.

R. D. Cheverton, S. K. Iskander, and D. G. Ball, Union Carbide Corp. Nuclear Div., Oak Ridge Natl. Lab., Oak Ridge, Tenn., *PWR Pressure Vessel Integrity During Overcooling Accidents: A Parametric Analysis*, NUREG/CR-2895 (ORNL/TM-7931), February 1983.

J. G. Merkle, Union Carbide Corp. Nuclear Div., Oak Ridge Natl. Lab., Oak Ridge, Tenn., *An Examination of the Size Effects and Data Scatter Observed in Small Specimen Cleavage Fracture Toughness Testing*, NUREG/CR-3672 (ORNL/TM-9088), April 1984.

W. R. Corwin, Martin Marietta Energy Systems, Inc., Oak Ridge Natl. Lab., Oak Ridge, Tenn., *Assessment of Radiation Effects Relating to Reactor Pressure Vessel Cladding*, NUREG/CR-3671 (ORNL-6047), July 1984.

W. R. Corwin, R. G. Berggren, and R. K. Nanstad, Martin Marietta Energy Systems, Inc., Oak Ridge Natl. Lab., Oak Ridge, Tenn., *Charpy Toughness and Tensile Properties of a Neutron Irradiated Stainless Steel Submerged-Arc Weld Cladding Overlay*, NUREG/CR-3927 (ORNL/TM-9709), September 1984.

J. J. McGowan, Martin Marietta Energy Systems, Inc., Oak Ridge Natl. Lab., Oak Ridge, Tenn., *Tensile Properties of Irradiated Nuclear Grade Pressure Vessel Plate and Welds for the Fourth HSST Irradiation Series*, NUREG/CR-3978 (ORNL/TM-9516), January 1985.

J. J. McGowan, Martin Marietta Energy Systems, Inc., Oak Ridge Natl. Lab., Oak Ridge, Tenn., *Tensile Properties of Irradiated Nuclear Grade Pressure Vessel Welds for the Third HSST Irradiation Series*, NUREG/CR-4086 (ORNL/TM-9477), March 1985.

W. R. Corwin, G. C. Robinson, R. K. Nanstad, J. G. Merkle, R. G. Berggren, G. M. Goodwin, R. L. Swain, and T. D. Owings, Martin Marietta Energy Systems, Inc., Oak Ridge Natl. Lab., Oak Ridge, Tenn., *Effects of Stainless Steel Weld Overlay Cladding on the Structural Integrity of Flawed Steel Plates in Bending, Series 1*, NUREG/CR-4015 (ORNL/TM-9390), April 1985.

N. J. Stelzman, R. G. Berggren, and T. N. Jones, Martin Marietta Energy Systems, Inc., Oak Ridge Natl. Lab. Oak Ridge, Tenn., *ORNL Characterization of Heavy-Section Steel Technology Program Plates 01, 02, and 03*, NUREG/CR-4092 (ORNL/TM-9491), April 1985.

G. D. Whitman, Martin Marietta Energy Systems, Inc., Oak Ridge Natl. Lab., Oak Ridge, Tenn., *Historical Summary of the Heavy-Section Steel*

Technology Program and Some Related Activities in Light-Water Reactor Pressure Vessel Safety Research, NUREG/CR-4489 (ORNL-6259), March 1986.

R. H. Bryan, B. R. Bass, S. E. Bolt, J. W. Bryson, J. G. Merkle, R. K. Nanstad, and G. C. Robinson, Martin Marietta Energy Systems, Inc., Oak Ridge Natl. Lab., Oak Ridge, Tenn., *Test of 6-in.-Thick Pressure Vessels. Series 3: Intermediate Test Vessel V-8A — Tearing Behavior of Low Upper-Shelf Material,* NUREG-CR-4760 (ORNL-6187), May 1987.

D. B. Barker, R. Chona, W. L. Fourney, and G. R. Irwin, University of Maryland, College Park, Md., *A Report on the Round Robin Program Conducted to Evaluate the Proposed ASTM Standard Test Method for Determining the Plane Strain Crack Arrest Fracture Toughness K_{Ia} of Ferritic Materials,* NUREG/CR-4966 (ORNL/Sub/79-7778/4), January 1988.

L. F. Miller, C. A. Baldwin, F. W. Stallman, and F. B. K. Kam, Martin Marietta Energy Systems, Inc., Oak Ridge Natl. Lab., Oak Ridge, Tenn., *Neutron Exposure Parameters for the Metallurgical Test Specimens in the Fifth Heavy-Section Steel Technology Irradiation Series Capsules,* NUREG/CR-5019 (ORNL/TM-10582), March 1988.

J. J. McGowan, R. K. Nanstad, and K. R. Thoms, Martin Marietta Energy Systems, Inc., Oak Ridge Natl. Lab., Oak Ridge, Tenn., *Characterization of Irradiated Current-Practice Welds and A533 Grade B Class 1 Plate for Nuclear Pressure Vessel Service,* NUREG/CR-4880 (ORNL-6484/V1 and V2), July 1988.

R. D. Cheverton, W. E. Pennell, G. C. Robinson, and R. K. Nanstad, Martin Marietta Energy Systems, Oak Ridge Natl. Lab., Oak Ridge, Tenn., *Impact of Radiation Embrittlement on Integrity of Pressure Vessel Supports for Two PWR Plants,* NUREG/CR-5320 (ORNL/TM-10966), February 1989.

J. G. Merkle, Martin Marietta Energy Systems, Inc., Oak Ridge Natl. Lab., Oak Ridge, Tenn., *An Overview of the Low-Upper-Shelf Toughness Safety Margin Issue,* NUREG/CR-5552 (ORNL/TM-11314), August 1990.

R. D. Cheverton, T. L. Dickson, J. G. Merkle, and R. K. Naastad, Martin Marietta Energy Systems, Inc., Oak Ridge Natl. Lab., Oak Ridge, Tenn., *Review of Reactor Pressure Vessel Evaluation Report for Yankee Rowe Nuclear Power Station (YAEC No. 1735),* NUREG/CR-5799 (ORNL/TM-11982), March 1992.

Acknowledgments

Nomenclature

a_o lattice parameter

b magnitude of Burgers vector

d_g grain diameter

f_{id} fraction of cascade interstitial that collapse into clusters

f_{vd} fraction of cascade vacancies that collapse into clusters

$z^j_{i,v}$ combinatorial number for interstitials or vacancies diffusing to a cluster of size j

$C_{i,v}$ atomic concentration of interstitials or vacancies

C_j atomic concentration of interstitial cluster with j interstitials

C^e_v thermal equilibrium atomic vacancy concentration

$D_{i,v}$ diffusivity of interstitials or vacancies

E^i_j rate constant for interstitial emission from an interstitial cluster of size j

E^B_j binding energy of an interstitial to an interstitial cluster of size j

G shear modulus

G_{dpa} atomic displacement rate

$G_{i,v}$ interstitial or vacancy generation rate

R recombination coefficient

$S^k_{i,v}$ sink strength of type-k extended defect for interstitials or vacancies

$Z^d_{i,v}$ dislocation capture efficiency for interstitials or vacancies

$Z^j_{i,v}$ interstitial cluster capture efficiency for interstitials or vacancies

$\beta^j_{i,v}$ rate constant for interstitial or vacancies impingement on a cluster of size j

η cascade efficiency

γ surface energy

ρ_d dislocation density

Ω atomic volume

Modeling the Influence of Irradiation Temperature and Displacement Rate on Radiation-Induced Hardening in Ferritic Steels[*]

R. E. Stoller

Introduction

Neutron irradiation gives rise to a number of phenomena that have been extensively studied. These include void swelling, irradiation creep, solute segregation, and embrittlement. In many cases, the observed property change can be correlated with the radiation-induced or radiation-enhanced microstructural evolution that has occurred and a number of models have been developed to investigate and describe this microstructural evolution (Brailsford and Bullough, 1981) (Druce, 1990) (Lucas et al., 1985) (Mansur, 1978) (Mansur, 1979) (Odette, 1983) (Stoller and Odette, 1982) (Stoller and Odette, 1987a) (Stoller and Odette, 1987b) (Wolfer et al., 1977). The reaction rate theory is most commonly used in these models. This theoretical description of radiation damage has been most successfully applied to void swelling and irradiation creep (Brailsford and Bullough, 1981) (Mansur, 1978) (Mansur, 1979) (Stoller and Odette, 1982) (Stoller and Odette, 1987a) (Stoller and Odette, 1987b) (Wolfer et al., 1977). Such work has generally been concerned with irradiation conditions of relatively high doses [>1 displacement per atom (dpa)] and temperatures ($T > 300°C$). In this regime, the vacancies and interstitials rapidly come into equilibrium with the microstructure and it is safe to assume that the point defect concentrations are at their steady state values. The steady state regime has been thoroughly explored and, in certain limiting cases, analytical solutions to the rate equations have been obtained that describe the dependence of a phenomenon such

as swelling on the total dose or the displacement rate (Mansur, 1978) (Stoller and Mansur, 1990).

The work discussed here was undertaken to investigate the radiation-induced "matrix defect" that is believed to contribute to hardening and embrittlement in the ferritic steels used for light water reactor (LWR) components. Irradiation temperature and displacement rate were identified as two key variables to be explored. The direction of the investigation was influenced by two recent observations of greater-than-expected levels of radiation damage accumulation following low temperature neutron irradiation. In one case, high levels of irradiation creep were observed in several austenitic and ferritic alloys after irradiation at temperatures below 300°C (Grossbeck et al., 1990). The second case involved the pressure vessel of the High Flux Isotope Reactor (HFIR) at the Oak Ridge National Laboratory (ORNL), where accelerated embrittlement was observed after irradiation at 50°C (Nanstad et al., 1988). The displacement rate was a potentially significant variable in both of these cases and the irradiation temperatures were sufficiently low to warrant an investigation of point defect transient effects. Subsequent modeling and analysis of the low-temperature creep experiment indicated that the high creep rates could be attributed to the influence of the point defect transient (Stoller et al., 1992).

Therefore, a simple model was used to first conduct a detailed numerical analysis of the time (dose) dependence of the point defect concentrations for irradiation conditions characteristic of LWR pressure vessels and support structures. The fraction of point defects that are lost due to matrix recombination reactions was used as another metric for evaluating the influence of the point defect transient. The results showed that the reactor pressure vessel operating temperature of 288°C is near a threshold below which the use of the steady state analysis is

probably not appropriate (Stoller and Mansur, 1990). The influence of the displacement rate was also investigated in this transient regime. The dose rate dependence of the recombination fraction during the transient was observed to be the inverse of that observed at steady state.

As a result of these experimental and theoretical observations, it was determined that the assumption of steady state defect concentrations would not be used in the development of the subsequent model that was used to investigate matrix defect hardening. The model is described in detail below. The results obtained with this model indicate that both interstitial and vacancy type clusters could contribute significantly to reactor pressure vessel (RPV) and support structure embrittlement. The relative importance of the two types of defects is determined by the irradiation temperature and displacement rate. Finally, it is worth noting that the importance of the point defect transient was discussed in another context many years ago (Sharp and Foreman, 1968), but computing limitations prevented more analysis at that time. It remained impractical to try to carry out the type of calculations discussed here until vastly improved computers became generally available over about the last five to ten years.

Description of Point Defect Kinetics and Theoretical Models

A basic description of point defect kinetics and the reaction rate theory will be given in this section. More details about the theory can be found in references such as Brailsford, 1981 and Mansur, 1978. The specific models used here build on earlier research that is described in detail in Stoller and Odette, 1982; Stoller and Odette, 1987a; Stoller and Odette, 1987b; and Stoller et al., 1992. That work investigated radiation effects at much higher temperatures and therefore applied the assumption of steady state point defect concentrations. Some details of the models, such as the calculation of the extended defect sink strengths (Brailsford and Bullough, 1981 and Stoller and Odette, 1982), are treated similarly in both cases.

Model Used to Investigate Point Defect Transient Effects

The equations describing the spatially averaged point defect concentrations can be written as:

$$\frac{dC_i}{dt} = G_i - RC_iC_v - D_iC_iS_i^T \qquad (1)$$

for the interstitial concentration, C_i, and

$$\frac{dC_v}{dt} = G_v - RC_iC_v - D_vC_vS_v^T \qquad (2)$$

for the vacancy concentration, C_v. The constants in Equations (1) and (2) are: G_i, the interstitial generation rate; G_v, the vacancy generation rate; R, the recombination rate coefficient; D_i, the interstitial diffusivity; and D_v, the vacancy diffusivity. The $S_{i,v}^T$ are the total sink strengths of all the extended defects in the material. These can include dislocations, grain boundaries and other interfaces, and the interstitial and vacancy clusters discussed below. In the general case, the interstitial and vacancy generation rates should include the displacement rate, G_{dpa}, and the point defects produced by thermal emission from extended defects. In addition, the dpa rate should be reduced by the cascade efficiency, η, to account for in-cascade recombination; and a term that accounts for in-cascade clustering fraction, f_{icl} and f_{vcl} (Diaz de la Rubia and Guinan, 1990; English et al., 1990; English et al., 1992; Diaz de la Rubia and Guinan, 1992). Thus the net point defect generation rates are given as:

$$G_{i,v} = \eta G_{dpa}(1 - f_{i,vcl}) + D_{i,v}\sum_j C_{i,v}^j S_{i,v}^j \qquad (3)$$

where the $S_{i,v}^j$ are the point defect sink strengths for extended defects of type j and the $C_{i,v}^j$ are the point defect concentrations in equilibrium with these defects. The interstitial formation energy is sufficiently high that the C_i^j can be neglected in

practice and even vacancy emission is small at the temperatures of interest to this work. The model does assume that interstitial emission can occur from small interstitial clusters, but discussion of the point defect clustering model will be deferred to the next section. The point defect clustering fractions were set to zero for the initial purpose of elucidating the effects of the point defect transient.

The microstructure of unirradiated pressure vessel steels is quite complex, including dislocations and a variety of precipitates and interfaces that form during heat treating. These interfaces can include the prior austenite grain boundaries, ferrite-bainite boundaries, and bainite-bainite packet boundaries. Such extended defects can act as both sources of and sinks for point defects in these materials. While it is not possible to model this microstructure in great detail, experience with void swelling and creep indicates that models that incorporate a modest level of microstructural information can achieve a very successful simulation of radiation damage (Brailsford and Bullough, 1981; Mansur, 1978; Mansur, 1979; Stoller et al., 1992; Stoller and Odette, 1982; Stoller and Odette, 1987a; and Stoller and Odette, 1987b; Wolfer et al., 1977). In the present work, the sink structure includes the dislocation network; a single, effective grain size to account for the various boundaries; and the radiation-induced point defect clusters. Both the grain size and dislocation density are assumed to remain unchanged during irradiation (Van Duysen et al., 1992).

The sink strengths of the extended defects are calculated only to lowest order (Brailsford and Bullough, 1981; Stoller and Odette, 1982). In this case, the dislocation sink strength for interstitials and vacancies is

$$S_{i,v}^d = Z_{i,v}^d \rho_d \tag{4}$$

where ρ_d is the dislocation density (m^{-2}) and the $Z_{i,v}^d$ are the point defect capture efficiencies. The grain boundary sink strength is a function of both the grain diameter, d_g, and the other sinks in the system,

$$S_g = \frac{6S_o^T}{d_g} \tag{5}$$

where S_o^T is the total vacancy sink strength of all the other sinks. The use of Equation (5) ignores the fact that the total system sink strength for interstitials is different from that for vacancies and that this would lead to the grain boundary interstitial sink strength being slightly different from the grain boundary vacancy sink strength (Brailsford and Bullough, 1981). This difference is negligible for the work discussed here. Equations (4) and (5) lead to the total sink strength that is used in Equations (1) and (2),

$$S_{i,v}^T = S_{i,v}^d + S_g + S_{i,v}^{ici} + S_{i,v}^{vci} \tag{6}$$

The interstitial ($S_{i,v}^{ici}$) and vacancy ($S_{i,v}^{vci}$) cluster sink strengths in Equation (6) will be given below. Both the dislocations and the grain boundaries are assumed to be in thermal equilibrium, so that the C_v^d and C_v^g terms needed for Equation (3) are set equal to the equilibrium vacancy concentration, C_v^e.

Description of Point Defect Clustering Model

Recent advances in the use of molecular dynamics (MD) simulations have provided more insight into the details of primary defect production (English et al., 1990; English et al., 1992; Diaz de la Rubia and Guinan, 1990; and Diaz de la Rubia and Guinan, 1992). Two observations from the MD work are particularly relevant to this study. First, only a fraction of the initially produced atomic displacements survive in-cascade recombination that occurs from about 1 to 10 ps after the cascade is created. This is reflected in the cascade efficiency term used in Equations (1) and (2). Second, a large fraction of the surviving defects are found in clusters, rather than as individual defects. This is accounted for by the in-cascade clustering fractions in these same equations. Both the cascade efficiency

and the clustering fractions are dependent on the energy of the primary knock-on atom (PKA) that creates the cascade. In principle, some spectrally averaged value of these parameters could be computed for a given material and neutron energy spectrum. The values used in these simulations do not represent such an average, but they are consistent with the MD results.

While both interstitial and vacancy clustering are treated in the model, more detail has been included in the interstitial component to date. Interstitial clusters with sizes up to a tetra-interstitial can form directly in the cascade, or essentially classical interstitial cluster nucleation can occur due to random collisions between diffusing defects. The in-cascade cluster fraction, f_{ict} is the sum of three components: the fraction forming di- (f_{ict}^2), tri- (f_{ict}^3), and tetra-interstitials (f_{ict}^4). Larger interstitial clusters are observed in MD simulations (English et al., 1990; English et al., 1992; Diaz de la Rubia and Guinan, 1992) but the model does not currently simulate their formation.

The evolution of the interstitial cluster population is given by a family of equations describing the reactions between immobile clusters and mobile point defects.

$$\frac{dC_2}{dt} = \eta G_{dpa} \frac{f_{ict}^2}{2} + \beta_i^1 \frac{C_1}{2} + (\beta_v^3 + E_i^3)C_3 - (\beta_v^2 + \beta_i^2 + E_i^2)C_2$$

(7)

for di-interstitials,

$$\frac{dC_3}{dt} = \eta G_{dpa} \frac{f_{ict}^3}{3} + \beta_i^2 C_2 + (\beta_v^4 + E_i^4)C_4 - (\beta_v^3 + \beta_i^3 + E_i^3)C_3$$

(8)

for tri-interstitials,

$$\frac{dC_4}{dt} = \eta G_{dpa} \frac{f_{ict}^4}{4} + \beta_i^3 C_3 + \beta_v^5 C_5 - (\beta_v^4 + \beta_i^4 + E_i^4)C_4$$

(9)

for tetra-interstitials, and

$$\frac{dC_j}{dt} = \beta_i^{j-1} C_{j-1} + \beta_v^{j+1} C_{j+1} - (\beta_v^j + \beta_i^j)C_j$$

(10)

for interstitial-clusters from size five up to the maximum. The rate constants for interstitial and vacancy impingement on an interstitial cluster of size j can be written as:

$$\beta_{i,v}^j = \frac{z_{i,v}^j}{a_o^2} D_{i,v} C_{i,v}$$

(11)

and the rate constant for interstitial emission from a cluster of size j is:

$$E_i^j = \frac{D_i}{a_o^2} \exp\left(\frac{-E_j^B}{kT}\right)$$

(12)

where E_j^B is the binding energy of an interstitial to a cluster of size j and a_o is the lattice parameter. Other calculations indicate that interstitial emission from clusters larger than the tetra-interstitial would be negligible at the temperatures of interest here (Ingle et al., 1981). Therefore, such emission is neglected in this work.

The $z_{i,v}^j$ in Equation (11) are combinatorial numbers, determined by the number of adjacent atomic sites from which an interstitial or vacancy can jump onto an interstitial cluster of size j. The combinatorial numbers can be computed for single defects and small clusters (Beeler, Jr. and Johnson, 1967; Johnson, 1979; Leffers and Singh, 1981), but it is difficult to determine these values for large clusters.

A continuum approach is typically used to describe point defect absorption by larger clusters, where an appropriate diffusion problem is solved to calculate a capture efficiency for the cluster (Wolfer and Ashkin, 1975) and this is used to compute the rate of point defect absorption. In this work, the interstitial clusters were assumed to be planar defects, i.e., dislocation loops, and the continuum rate constants analogous to Equation (1) are:

$$\beta'_{i,v} = \frac{2\pi r_i(j)}{\Omega} D_{i,v} C_{i,v} Z^t_{i,v}(j) \qquad (13)$$

where $r_i(j)$ and $Z_{i,v}{}^t(j)$ are the radius and capture efficiency of a loop comprised of j interstitials and Ω is the atomic volume. By equating Equations (11) and (13), an effective capture efficiency was calculated. This calculation was done subject to two constraints. The first was that the interstitial and vacancy capture efficiencies for large loops should asymptotically approach the values used for the dislocation network. The second constraint was that the calculated capture efficiency for a single interstitial should be the same as that determined by the atomistic, combinatorial method. With this approach, the only combinatorial numbers needed are those for a single interstitial or vacancy combining with an interstitial. Based on earlier experience (Stoller and Odette, 1987b) and values in the literature (Beeler, Jr. and Johnson, 1967; Johnson, 1979; Leffers and Singh, 1981), the nominal values used were: $z_i^1 = 56$ and $z_v^1 = 42$. Between the determined lower and upper limits, the capture efficiency was assumed to be proportional to the reciprocal of the square of the cluster radius (Wolfer and Ashkin, 1975).

As mentioned above, vacancy clustering is presently treated in less detail than is interstitial clustering. Vacancy cluster formation is assumed to happen only as the result of cascade collapse. The clusters are assumed to form directly in the cascade as microvoids with a radius r_{vcl}. The vacancy cluster generation rate, G_{vcl} is determined by the fraction of the vacancies that are assumed to collapse into the clusters and the number of vacancies per cluster, n_v

$$G_{vcl} = \eta f_{vcl} \frac{G_{apa}}{\Omega n_v} \qquad (14)$$

$$n_v = \frac{4\pi}{3\Omega} r_{vcl}^3 \qquad (15)$$

For the irradiation conditions of interest here, these microvoids are generally unstable and shrink at a rate determined by the relevant point defect fluxes,

$$\frac{dr_{vcl}}{dt} = \frac{1}{r_{vcl}} \left(D_v C_v - D_i C_i - D_v C_v^{vcl} \right) \qquad (16)$$

where $C_v{}^{vcl}$ is the vacancy concentration in equilibrium with the microvoid.

$$C_v^{vcl} = C_v^e \exp \left(\frac{2\gamma\Omega}{r_{vcl} kT} \right) \qquad (17)$$

in which γ is the surface free energy and C_v^e is the thermal equilibrium vacancy concentration. The mean vacancy cluster lifetime, τ_{vcl} is obtained by integrating Equation (16) from the initial size down to the size at which only a single vacancy remains,

$$\tau_{vcl} = \int_{r_{vcl}}^{r(1)} \left(\frac{dr_{vcl}}{dt} \right)^{-1} dr_{vcl} \qquad (18)$$

Using Equations (14) through (18), the time-dependent rate equation for the vacancy cluster density, N_{vcl} is (Stoller and Odette, 1982):

$$\frac{dN_{vcl}}{dt} = G_{vcl} - N_{vcl} \tau_{vcl}^{-1} \qquad (19)$$

Hardening Due to Point Defect Clusters

A dislocation barrier model has been used to calculate the matrix hardening due to the interstitial and vacancy clusters. As discussed by Bement (Bement, Jr., 1970), such models are typically derived from the theory developed by Orowan to describe hardening due to precipitates and involve a calculation of the shear stress required to move a dislocation through an obstacle in its glide plane. An incremental change in the yield stress can be related to this shear stress. In its simplest form, the change in the shear stress, $\Delta\tau$, can be written as:

$$\Delta\tau = \frac{Gb}{\beta\bar{\ell}} \qquad (20)$$

in which G is the shear modulus and b is the magnitude of the Burgers vector. The average barrier spacing, $\bar{\ell}$, is computed from the number density, N, and the diameter, d, of the obstacles, $\bar{\ell} = (Nd)^{-1/2}$. The factor β in Equation (20) is a function of the barrier strength. For example, $\beta = 1$ for a periodic array of strong barriers, such as incoherent precipitates (Bement, Jr., 1970). Either the Tresca or Von Mises yielding criterion can be used to convert the calculated shear stress to a change in the uniaxial yield stress, in either case, $\Delta\sigma_y = 2\Delta\tau$ (Dieter, 1976).

A number of potential values for the barrier strength term in Equation (20) are discussed in Bement, Jr., 1970. Depending on the barrier model chosen, the calculated hardening due to a specific type of obstacle can vary by more than a factor of 100. For example, if interstitial loops are assumed to be strong barriers, $\beta = 3 - 4$ in the Orowan model. Alternately, a weak barrier model that incorporates Friedel's effective barrier spacing gives:

$$\Delta\tau = \frac{Gb}{\beta}dN^{1/2} \qquad (21)$$

with $\beta = 8$ for body-centered-cubic materials (Bement, Jr., 1970). A comparison of Equation (20)

with $\beta = 3$ and Equation (21) is shown in Figure 1. The results shown in Figure 1 reflect loop densities of 1×10^{20} and 1×10^{22} m^{-3}. The difference between the two models is greater for smaller loops and for lower number densities. The figure includes a similar comparison for voids. In the case of voids, $\beta = 1$ in the Orowan (strong barrier) model. If Friedel's model is invoked for voids, the radius is used in Equation (21) instead of the diameter and $\beta = 10$. The calculated hardening due to voids is more sensitive to the choice of barrier model than is the case for loops. A model proposed by Weeks, et al. (Weeks et al., 1969) leads to values that lie between these two cases. The three void strengthening models are compared in Figure 2. The influence of the uncertainties related to the various barrier models will be discussed further below.

Results of Calculations

The major material and irradiation parameters used in these calculations are listed in Table 1. The range of displacement rate values includes those characteristic of accelerated test reactor irradiations and power reactor surveillance and support structure locations. Where possible, the values of the material parameters represent best estimates obtained from the literature (Hettich et al., 1977; Murr, 1975; and Schaefer et al., 1977). For some parameters, where it was difficult to determine a "best" value, a range of values was used to determine the sensitivity of the calculations to these parameters. The microstructural parameters such as the dislocation density and grain size were similarly varied within the range of values found in the literature (Odette and Lucas, 1989; and Van Duysen et al., 1992).

Calculation of Point Defect Transients and Steady State Point Defect Concentrations

The time dependence of the point defect concentrations is primarily determined by the displacement rate, the matrix recombination coefficient, and the sink structure. Three characteristic times can be derived from Equations (1) and (2) if the equations are solved simultaneously for two limiting cases (Mansur, 1978; Sharp and Foreman, 1968; and Stoller and Mansur, 1990). The cases are: (1) no point defects are
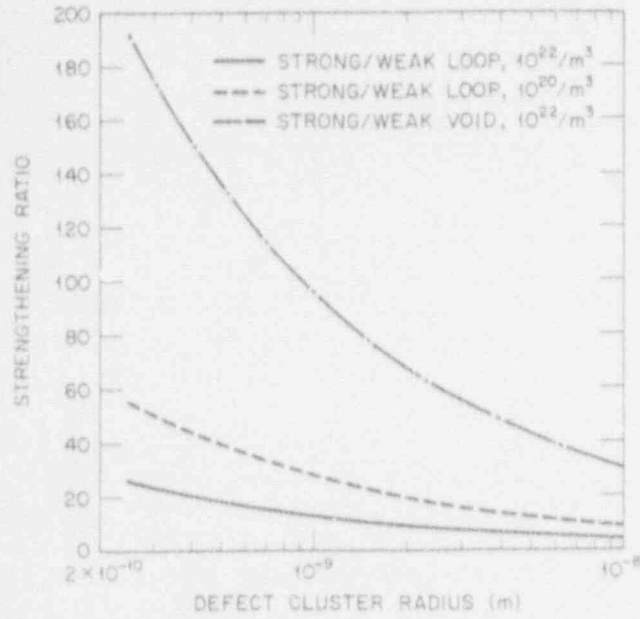
Figure 1. Ratio of strengthening values obtained with "strong" and "weak" barrier models (Bement, Jr., 1970) for interstitial loops and voids.
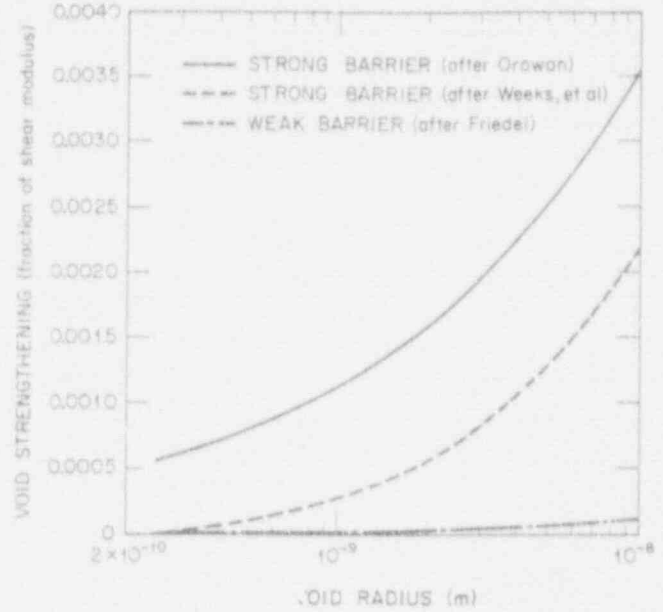
Figure 2. Comparison of void strengthening values obtained with various models (Bement, Jr., 1970). Void number density is 1×10^{22} m^3.

Table 1. Typical irradiation and material parameters

Irradiation temperature (°C)	60 to 283
Displacement rate (dpa/s)	1.0×10^{-11} to 1.0×10^{-3}
Cascade efficiency	0.1
Interstitial clustering fraction	0.0 to 0.6
Interstitial cluster binding energies (eV) di, tri, and tetra interstitial	0.5, 0.75, 1.25
Vacancy clustering fraction	0.0 to 0.6
Vacancy cluster radius (nm)	0.25 to 1.0
Pre-exponential, vacancy diffusivity (m²/s)	5.0×10^{-6}
Interstitial migration energy (eV)	1.25
Pre-exponential, vacancy diffusivity (m²/s)	5.0×10^{-5}
Vacancy migration energy (eV)	1.25
Vacancy formation energy (eV)	1.55
Lattice parameter (nm)	0.287
Recombination radius (nm)	0.574 to 1.15
Surface free energy (J/m²)	$2.947 - 4.5 \times 10^{-4} * T(°C)$
Interstitial-dislocation capture efficiency	1.00
Network dislocation density (m²)	1.0×10^{13} to 1.0×10^{15}
Effective grain size (μm)	10. to 1000.

absorbed at sinks and (2) no matrix recombination. While both cases are mathematically well defined, behavior at these limits is unlikely to occur in practice. The sink structure will determine the degree to which point defect absorption is dominated by either matrix recombination $(RC_i >> D_v S_v^T)$ or by absorption at sinks $(D_v S_v^T >> RC_i)$. The simple solutions discussed below assume equal point defect generation rates, i.e., no thermal emission of point defects from sinks and no in-cascade clustering. The use of the term "steady state" in this discussion implies that the sink structure is not changing significantly while the point defect concentrations are evolving. This approximation is not always physically reasonable, but it is useful here for purposes of explanation.

The first time of interest is that required for the point defect concentrations to reach a sufficiently high value for matrix recombination to limit their further increase, τ_R. If the point defect losses were completely dominated by matrix recombination, i.e., no point defects were absorbed at sinks, then τ_R would determine the time to steady state,

$$\tau_R = (R\eta G_{dpa})^{-\frac{1}{2}} \qquad (22)$$

If there is a finite loss of point defects to sinks (as is usually the case), then the time required for the vacancies to diffuse to sinks, τ_v, is the time that determines the approach to steady state,

$$\tau_v = \left(D_v S_v^T \right)^{-1} \qquad (23)$$

The time for interstitials to diffuse to sinks, τ_i, is typically much shorter than τ_v because of the higher interstitial diffusivity,

$$\tau_i = \left(D_i S_i^T \right)^{-1} \qquad (24)$$

Similarly, the steady state point defect concentrations can be derived from the time-independent

versions of Equations (1) and (2) for these same two limiting cases. For times less than the minimum of that defined by Equation (22) or (24), the point defect concentrations build up linearly and $C_i = C_v = \eta G_{dpa} t$. For the completely matrix recombination dominated case, this behavior persists until the point defect concentrations reach steady state at τ_R, where

$$C_i^{ss} = C_v^{ss} = \left(\frac{\eta G_{dpa}}{R} \right)^{\frac{1}{2}} \qquad (25)$$

$C_i = C_v$ at steady state since their production rates are equal and they are only lost by mutual annihilation. For the sink-dominated case, the interstitial and vacancy concentrations again build up linearly and reach their steady state values at τ_i and τ_v, respectively. In this case the steady state concentrations are

$$C_{i,v}^{ss} = \frac{\eta G_{dpa}}{D_{i,v} S_{i,v}^T} \qquad (26)$$

For a case in which point defects are lost by both absorption at sinks and matrix recombination, the point defect concentrations initially build up in a manner similar to the recombination dominant case, i.e., $C_i(t) = C_v(t)$. If $\tau_i < \tau_R$ this behavior persists until the interstitials begin to be lost to sinks at τ_i. At that point, the interstitial concentration reaches a pseudo-steady state value which is determined by the sink strength and remains at that value while the vacancy concentration continues to increase up to τ_v. As the vacancy concentration approaches steady state, the interstitial concentration begins to decrease due to matrix recombination and both point defect populations reach their true steady state values. The behavior is somewhat different if $\tau_i > \tau_R$. In this case, the interstitial and vacancy populations reach the same pseudo-steady state value which is determined by the matrix recombination rate. These concentrations are maintained until τ_i, at which time the interstitial concentration begins to decrease as they are lost at sinks. The vacancy concentration increases as a result. At τ_v, the vacancies begin to be

lost to sinks and both the interstitial and vacancy concentrations reach their true steady state.

The relationship of the point defect concentrations and the characteristic times defined in Equations (22) to (24) are shown in Figure 3 for three of the cases of point defect absorption just discussed. The temperatures and displacement rate used to prepare Figure 3 are representative of LWR pressure vessels and support structures and the individual steady state times (τ_R, τ_s, and τ_i) for each case are indicated on the abscissa. To limit the number of curves in the figure, the case for which $\tau_i > \tau_R$ is not included. In order to demonstrate the behavior at the true recombination dominated limit denoted by R, an non-physical value of zero is required for the dislocation sink strength. The dislocation sink strengths for the other two cases were: 1×10^{11} and 1×10^{14} m^{-2} for the mixed-absorption case denoted by M and the sink dominated case denoted by S, respectively.

Note that the curve marked S at 60°C does not demonstrate sink dominated behavior because the same sink strengths were used at both temperatures. As shown in the figure, the point defect concentrations reach much higher levels at 60°C than at 285°C due to their reduced mobility at the lower temperature. This leads to a higher matrix recombination rate for a given sink strength. As a result, although a sink strength of 1×10^{14} m^{-2} is sufficient to demonstrate sink dominated behavior in Figure 3(a), this same value leads to a mixed absorption case at 60°C. For the case denoted M at 60°C, τ_s is greater than maximum value on the abscissa and the steady state has not been achieved.

The time required for the vacancies to diffuse to sinks is what limits the approach to steady state. This time is shown in Figure 4 as a function of temperature for two values of the dislocation sink strength. For engineering materials, the higher dislocation density is more relevant. However, the dependence on the sink strength implies that more attention should be paid to characterizing the microstructure of materials used in surveillance programs and test reactor irradiation experiments. Although only the dislocation density was varied to obtain the results shown in this figure, it is the total system sink strength that determines τ_s in Equation (23). This includes grain boundaries and

other internal interfaces, such as bainite packet boundaries. Thus, microstructural differences between engineering materials and the simple model alloys that are frequently used to investigate embrittlement mechanisms could significantly alter point defect behavior.

The very strong temperature dependence and long times observed below 300°C in Figure 4 indicate that models which invoke the assumption of steady state point defect concentrations to analyze low temperature embrittlement data may be suspect. Fairly modest differences in irradiation temperature between different experiments could confound data correlation and even limited temperature extrapolations in this domain need to consider the potential influence of the transient. The time dependence of the point defect concentrations at 60 and 285°C for a physically reasonable dislocation density of 1×10^{14} m^{-2} are compared in Figure 5 to highlight this point. Two major differences are observed. The first is that the vacancy concentration reaches steady state after about 100 seconds at 285°C, but not until after almost 30 years at 60°C. This result is particularly significant for the conditions of the HFIR pressure vessel (Nanstad et al., 1988) since it means that the entire irradiation has been conducted within the point defect transient regime.

The second difference observed in Figure 5 is a result of the greater matrix recombination at 60°C than at 285°C. As discussed above, a sink strength of 1×10^{14} m^{-2} is sufficient to yield sink dominated behavior at 285°C, but not at 60°C. The interstitial concentration reaches steady state at about 1×10^{-7} s at 285°C and remains essentially constant as the vacancy concentration approaches steady state. In this case, the primary effect of the transient is the existence of a short period during which the vacancy concentration is below its steady state value. The situation is similar for the vacancies at 60°C, but quite different for the interstitials. The contribution of matrix recombination leads to an extended period ($\sim 10^{-7}$ s to 10^{9} s) during which the interstitial concentration is much higher than its steady state value. This interstitial supersaturation would enhance the formation of interstitial clusters and influence the evolution of all defect structures that respond to a flux of interstitials (Grossbeck et al., 1990 and Stoller et al., 1992).
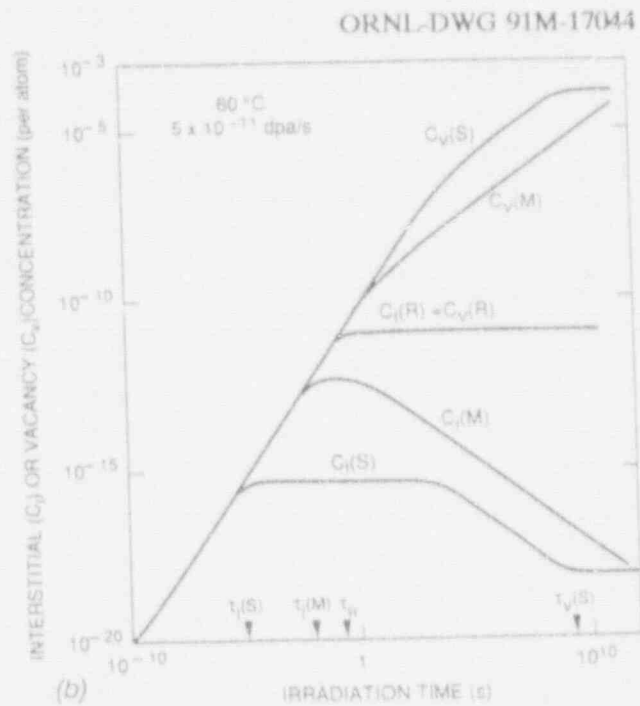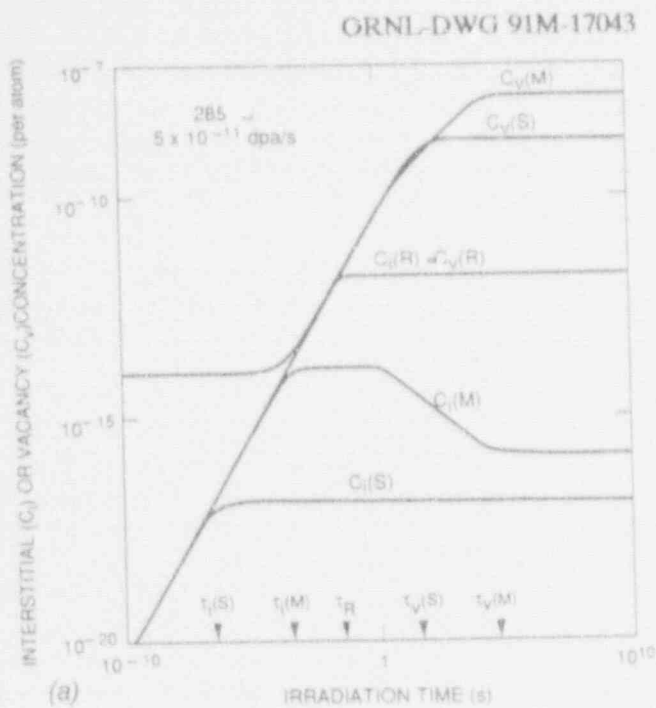
Figure 3. Time dependence of the interstitial and vacancy concentrations at 285 (a) and 60°C (b) for matrix recombination-dominanted (R) defect absorption, sink-dominated (S) point defect absorption, and a case of mixed (M) recombination and absorption at sinks. See text for sink strength values.
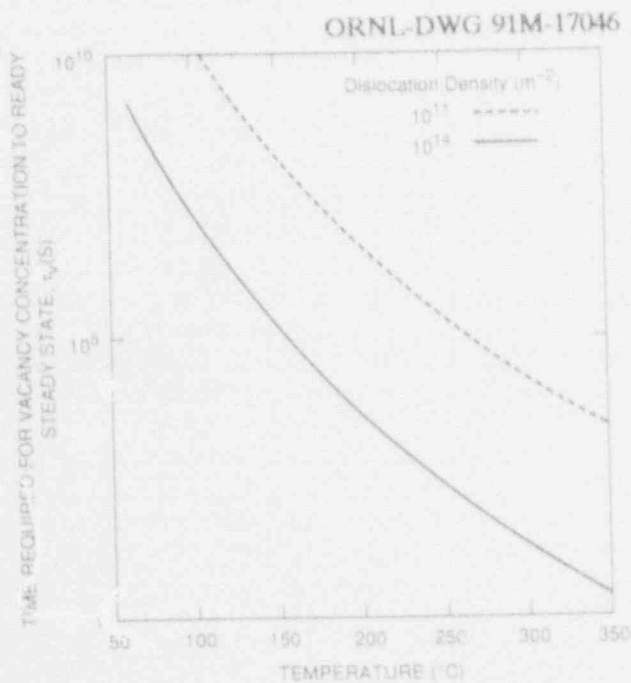
Figure 4. Time required for the vacancy concentration to reach steady state as a function of temperature for the indicated dislocation sink strength.
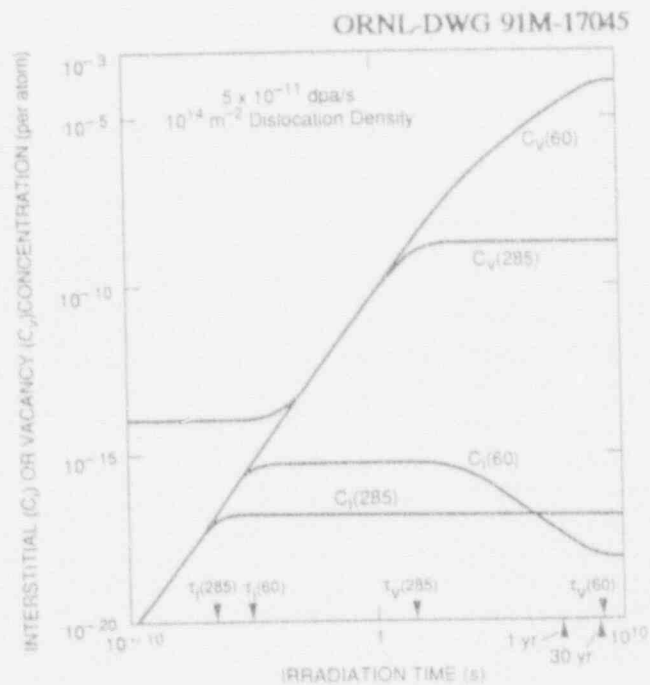
Figure 5. Time dependence of the point defect concentrations at 60 and 285°C for typical sink strengths but without point defect clustering.

The results shown in Figures 3 through 5 neglected point defect clustering, but similar results are obtained when clustering is included in the calculations. The impact of including the clustering model discussed above can be seen by comparing Figure 6 with Figure 5. The major effect is to simply reduce the point defect concentrations at any given time. This comes about for two reasons. First, the effective generation rates of freely migrating interstitials and vacancies are reduced by in-cascade clustering. Then, more of the migrating point defects are absorbed by the defect clusters which act as sinks. The effects of the point defect transient shown in Figure 5 are not significantly modified by the presence of the point defect clusters.

The competition between matrix recombination and absorption at sinks can also be observed in the displacement rate and temperature dependence of the steady state point defect concentrations as shown in Figures 7 and 8. At 60°C, for a fixed dislocation density of 1×10^{14} m^{-2}, the steady state point defect concentrations are proportional to the square root of the displacement rate for displacement rates in the range of 1×10^{-11} to 1×10^{-7} dpa/s. This is characteristic of recombination dominated behavior. However, the behavior is more complex at 285°C. For low displacement rates, near those of LWR pressure vessels, the point defect concentrations are linearly proportional to the displacement rate. This is the expected behavior for sink-dominated point defect absorption. However, the higher point defect concentrations that are obtained as the displacement rate increases eventually lead to more matrix recombination. Thus, at damage rates typical of test reactor irradiations, the dependence on displacement rate at 285°C approaches the square root dependence observed at 60°C. A change in slope can be seen in the 285°C curves near 10^{-9} dpa/s in Figure 7.

The temperature dependence of the point defect concentrations in Figure 8 can be similarly understood. As the temperature is decreased, the vacancy concentration increases due to a lower mobility. Higher vacancy concentrations lead to lower interstitial concentrations as long as the system sink strength is low enough for point defect absorption to be recombination dominated. In Figure 8, this situation is maintained at all

temperatures for a dislocation density of 1×10^{11} m^{-2} and at temperatures below about 200°C for a dislocation density of 1×10^{14} m^{-2}. For the higher dislocation density and temperatures above 200°C, absorption by sinks is dominant and the higher interstitial mobility leads to greater absorption and lower concentrations.

It should once again be pointed out that the results shown in Figures 7 and 8 neglect point defect clustering. The fact that the point defect concentrations are reduced when clustering is included was mentioned above. Point defect clusters will increase the system sink strength and shift the transition points on the curves in these figures. For example, the transition from sink dominated to recombination dominated behavior shown at 285°C in Figure 7 would be shifted to higher displacement rates. By the same token, a region of sink dominated behavior could occur at 60°C for low displacement rates. The location of the calculated transitions is also strongly influenced by the diffusion parameters that are used in the calculations. However, the fact that such transitions in behavior can exist needs to be considered when data is extrapolated in either displacement rate or irradiation temperature.

Influence of the Point Defect Transient on Matrix Recombination

In this section, the number or fraction of point defects that are lost due to matrix recombination will be used as a measure of the influence of the displacement rate and irradiation temperature in the transient and steady state regimes. Although the choice of this parameter is somewhat arbitrary, the recombination fraction is a reasonable figure of merit since the point defects that escape recombination are those that provide a source for radiation-induced microstructural and mechanical property changes (Stoller and Mansur, 1990). For the sake of simplicity, the influence of point defect clustering is neglected in most of the results presented.

Recombination Fraction in Limiting Cases

The number of point defects that have been lost to matrix recombination up to some time, τ, can be calculated as:

Figure 6. Time dependence of the point defect concentrations at 60 and 285°C for typical sink strengths with point defect clustering included.
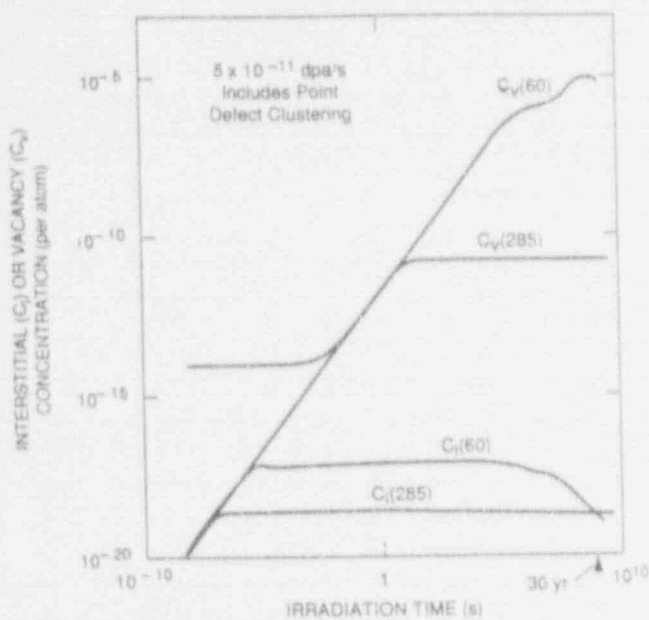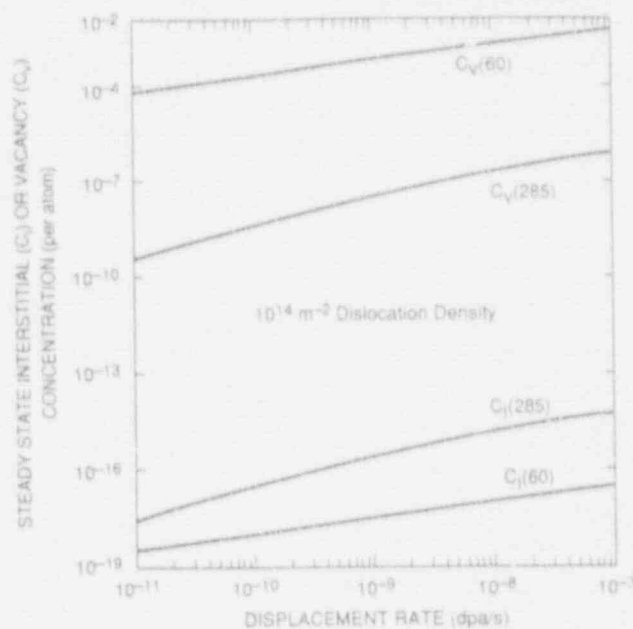
Figure 7. Displacement rate dependence of the steady state point defect concentrations at 60 and 285°C for typical sink strengths, point defect clustering not included.
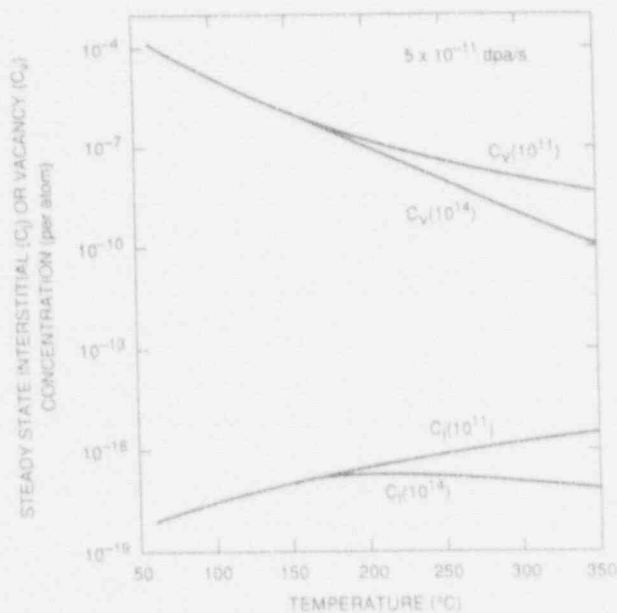
ORNL-DWG 91M-17048

Figure 8. Temperature dependence of the steady state point defect concentrations for LWR displacement rate and two values of the dislocation sink strength, point defect clustering not included.

$$N_R = \int_o^T R C_i C_v \, dt \qquad (27)$$

and the recombination fraction f_R can be found by dividing N_R by the total number of defects generated. The limiting values of C_i and C_v obtained during the linear transient and at steady state for both recombination and sink-dominated point defect absorption were given in the previous section. They are listed again in Table 2 along with the results of integrating Equation (27) for the three cases (Stoller and Mansur, 1990). These integrations can be carried out analytically for these limiting cases since the point defect concentrations are linear in time during the transient and independent of time at steady state. The term Δ used in Table 2 is an effective irradiation dose, $\Delta = \eta G_{dpa} \tau$, i.e., the total number of point defects that have survived in-cascade recombination. The dose and displacement rate terms have been grouped in this way to make it simple to extract both the dose dependence at a given displacement rate and the displacement rate dependence at a fixed dose.

The expressions listed in Table 2 can be used to provide an estimate for how the recombination fraction changes with the displacement rate (Stoller and Mansur, 1990). Alternately, the change in the irradiation time required to give equivalent recombination fractions at different displacement rates can be calculated. The dose dependence of the recombination fraction is seen to be quadratic at low doses, and dose-independent at high doses. For a given dose, recombination fraction is inversely proportional to the displacement rate during the transient. At steady state, the recombination fraction is linearly dependent on the displacement rate if the system is sink-dominated and independent of the displacement rate if it is recombination-dominated. These relationships hold as long as the system sink strength is not strongly affected by the displacement rate.

Recombination Fraction at Intermediate Doses

The number and fraction of point defects undergoing matrix recombination at doses between the limits just discussed was obtained by integrating

Equations (1) and (2) and summing the matrix recombination losses at each time step. The results obtained at 275°C for a range of displacement rates are shown in Figure 9. For the dislocation sink strength used here, 1×10^{15} m^{-2}, the defect absorption is sink-dominated for most of the curves shown in Figure 9(a) and the number of defects lost to recombination increases linearly with dose. At a fixed dose, the number recombining increases linearly with displacement rate. The fraction of the radiation-produced vacancies lost to recombination under these conditions is similarly plotted in Figure 9(b). For displacement rates less than 10^{-8} dpa/s, the recombination fraction is less than 10%. The recombination fraction increases with displacement rate because the interstitial and vacancy concentrations increase as listed in Table 2. Reference to Equations (1) and (2) shows that while the number of point defects lost to sinks increases linearly with C_i or C_v, the number recombining increases as their product.

To illustrate the range of observed behavior, additional results at lower doses for the same conditions as Figure 9 are shown in Figure 10. Consistent with the calculated limiting behavior listed in Table 2, the number recombining exhibits a cubic dose dependence at low doses and a linear dependence at high doses. At low doses, the number recombining is inversely proportional to the displacement rate. However, this dependence is reversed at high doses where the number recombining is proportional to the displacement rate. The transition between low-dose and high-dose behavior occurs near the vacancy diffusion time, τ_v. While the transition doses are very low at 285°C, these doses can be increased to significant levels at lower temperatures as a result of lower vacancy mobility. For example, the transition dose at 60°C is shown in Figure 11 to be greater than 1×10^{-4} dpa.

It has already been pointed out that for conditions that are strongly sink dominated ($G_{dpa} < 10^{-8}$), Figure 9 shows that the number of vacancies lost to recombination at a given dose increases linearly with displacement rate. As the fraction lost to recombination becomes significant at higher displacement rates, the dependence on displacement rate becomes weaker. This is expected from the values listed in Table 2 which show that there should be no dependence on displacement rate for

Table 2. Values of the interstitial (C_i) and vacancy (C_v) concentrations, and the number (N_R) and fraction (f_R) of point defects lost to matrix recombination for limiting cases ($f_{wd} = 0$ and no thermal vacancy emission)

	C_i	C_v	N_R	f_R
Linear transient	$\eta G_{dpa} \tau$	$\eta G_{dpa} \tau$	$\dfrac{R}{3} \dfrac{\Delta^3}{\eta G_{dpa}}$	$\dfrac{R}{3} \dfrac{\Delta^2}{\eta G_{dpa}}$
Steady state, recombination dominant	$\left(\dfrac{\eta G_{dpa}}{R}\right)^{1/2}$	$\left(\dfrac{\eta G_{dpa}}{R}\right)^{1/2}$	Δ	1
Steady state, sinks dominant	$\dfrac{\eta\, G_{dpa}}{D_i S_i^T}$	$\dfrac{\eta\, G_{dpa}}{D_v S_v^T}$	$\dfrac{R\, \eta\, G_{dpa}}{(D_i D_v S_i^T S_v^T)}\Delta$	$\dfrac{R\, \eta\, G_{dpa}}{(D_i D_v S_i^T S_v^T)}$

(a)

(b)

Figure 9. Displacement rate dependence of the number (a) and fraction (b) of vacancies lost to matrix recombination as a function of dose at 275°C. Dislocation sink strength is 1×10^{15} m^{-2}.
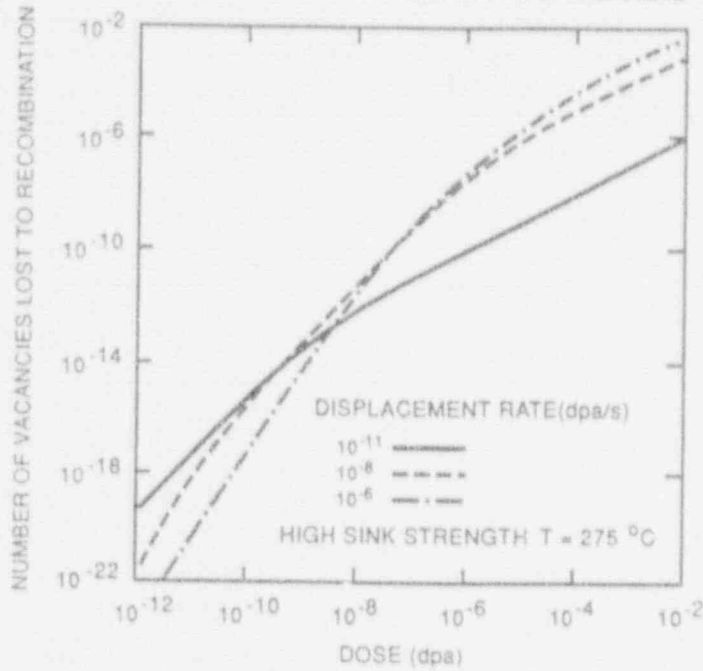
Figure 10. Displacement rate dependence of the number
of vacancies lost to matrix recombination as a
function of dose at 275°C for sink-dominant
conditions. Similar to Figure 9(a), but over
a larger dose range.

ORNL-DWG 90Z-10449
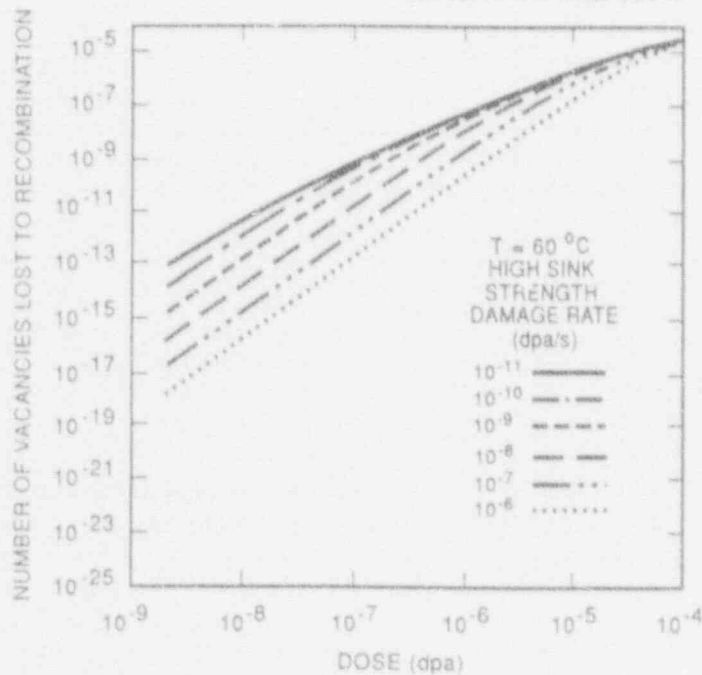
Figure 11. Displacement rate dependence of the number
of vacancies lost to matrix recombination as a
function of dose at 60°C. Dislocation sink
strength is 1×10^{15} m^{-2}.

15

conditions that are dominated by recombination. This result is illustrated in Figure 12 where the number and fraction of vacancies lost to recombination are shown as a function of dose for a low $(1 \times 10^{10}$ m$^2)$ dislocation sink strength. The number recombining initially increases at a cubic rate in Figure 12(a) and, at a given dose, the number is inversely proportional to the displacement rate. However, as the recombination fraction approaches 1.0 at the doses shown in Figure 12(b), the displacement rate dependence of the number recombining becomes linear and independent of displacement rate.

Influence of Displacement Rate and Temperature on Point Defect Recombination With Point Defect Clustering

When point defect clustering is included in the model calculations, the higher system sink strength contributed by the clusters tends to reduce the fraction of point defects that are lost to matrix recombination. Typical results obtained with the complete model are shown in Figures 13 and 14, where the cumulative fraction of the interstitials that have escaped matrix recombination $(1 - f_R)$ at a total dose of 0.01 dpa has been plotted as a function of the displacement rate and irradiation temperature. This dose was chosen because it is near the end-of-life for a LWR pressure vessel. The vacancy clustering fraction used in these calculations was 0.5, and the di-, tri-, and tetra-interstitial clustering fractions were 0.15, 0.1, and 0.05, respectively. The dislocation sink strength was 5×10^{14} m^2.

The results shown in Figure 13 for 60°C irradiation indicate that there is a transition from strong to weak displacement rate dependence at intermediate values of the displacement rate. Displacement rates typical of test reactor irradiations are in the region of weaker dependence. This indicates that extrapolations from data obtained in test reactor irradiation experiments could lead to misleading estimates of the effects to be expected at the much lower displacement rates that are characteristic of LWR components. Few point defects are lost to matrix recombination at 285°C at any displacement rate. This is quite different from the results shown earlier in Figure 9(b) when point defect clustering was not included in the calculations. In that figure, a large fraction of the point defects recombined for

displacement rates greater than about 1×10^{-8} dpa/s. This reduction in the fraction recombining is due to point defect absorption by the interstitial and vacancy clusters.

The temperature-dependent curves in Figure 14 similarly exhibit regions of strong and weak dependence. The results are only weakly temperature dependent above a threshold that is determined by the displacement rate. For a typical test reactor displacement rate, the threshold is about 150°C, while the threshold is at about 100°C for a LWR pressure vessel displacement rate. The temperature dependence is also steeper at the higher displacement rate. The potential for such shifts in temperature dependence also need to be considered when correlating or extrapolating embrittlement data. Figure 15 provides an additional example of how clustering influences the fate of point defects. The results shown in the figure were calculated using the same parameters as were used for Figure 14, but the point defect clustering fractions were set to zero. Much more recombination takes place in the absence of the clusters. The sensitivity of the calculations to the changes in the system sink strength induced by the point defect clusters indicates the importance of obtaining a good characterization of the microstructures that evolve under irradiation.

Predicted Strengthening Due to Point Defect Clusters

The behavior of the kinetic model developed for this work has been described in some detail. In order to investigate the strengthening that could be induced by point defect clusters, calculations were carried out using the complete model with the clustering fractions listed above. These values are consistent with the most recent MD simulations (English et al., 1990; English et al., 1992; and Diaz de la Rubia and Guinan, 1992). As discussed above, the predicted strengthening will be strongly dependent on the assumed barrier strength, and it is not clear which barrier model is most appropriate for the small clusters that are formed. Therefore, a simple Orowan-like model was used to calculate the strengthening. Both the interstitial loops and microvoids were assumed to be strong barriers, with $\beta = 3$ and $\beta = 1$, respectively. This approach should be adequate for the purpose of examining the
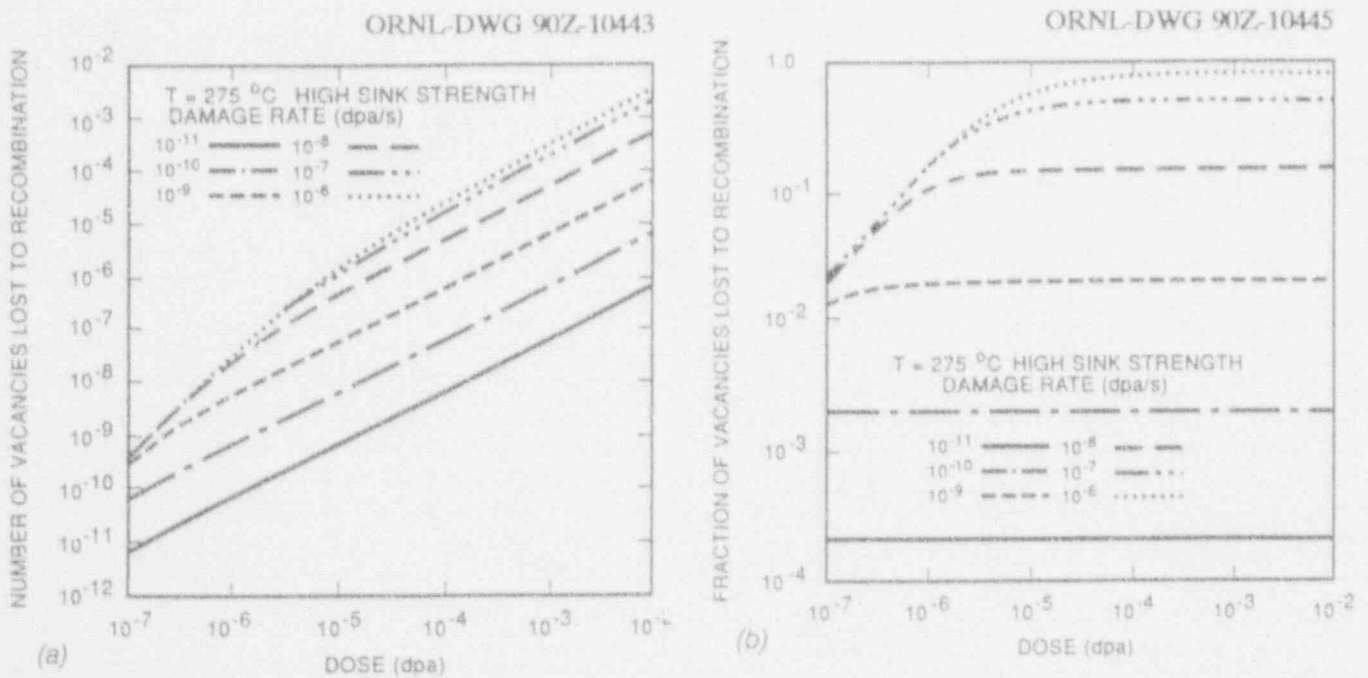
(a)

(b)
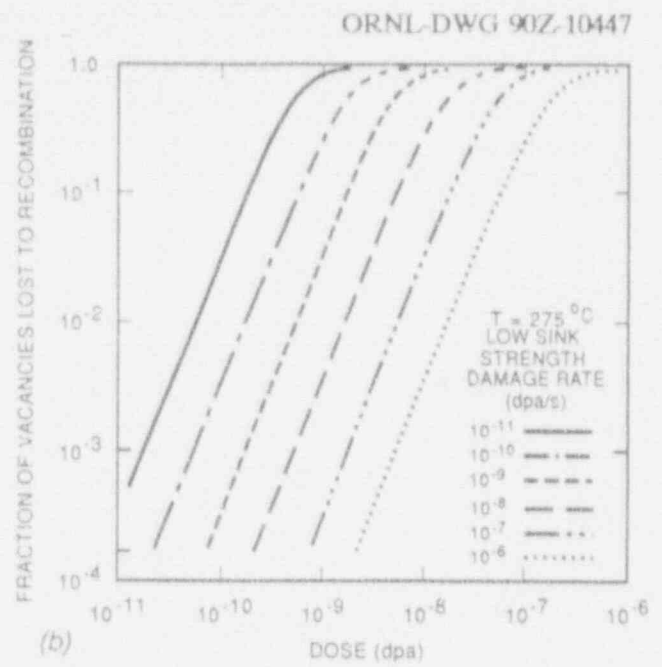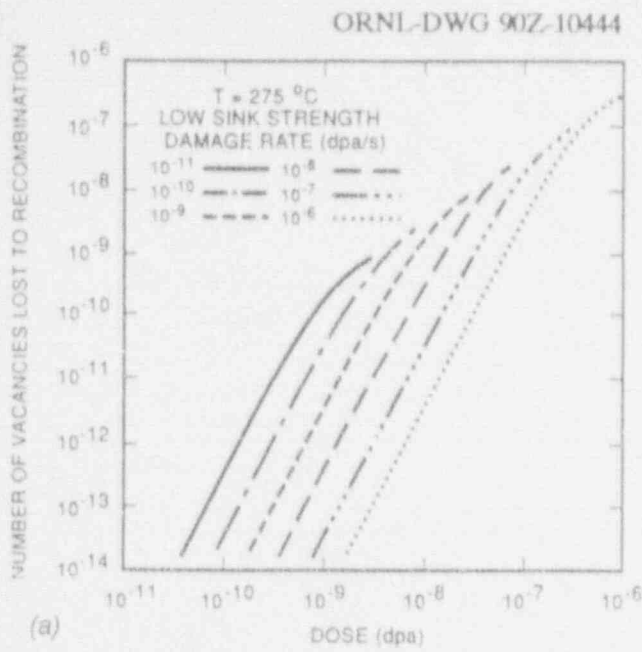
Figure 12. Displacement rate dependence of the number (a) and fraction (b) of vacancies lost to matrix recombination as a function of dose at 275°C. Dislocation sink strength is 1×10^{15} m^{-2}.

ORNL-DWG 92-5367

ORNL-DWG 92-5368
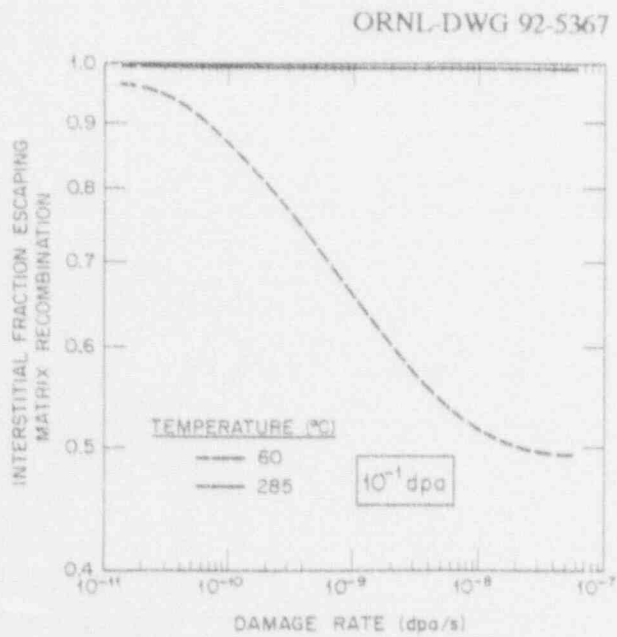
Figure 13. Influence of displacement rate on the fraction of interstitials lost to matrix recombination at a total dose of 0.1 dpa for irradiation temperatures of 60 and 285°C.
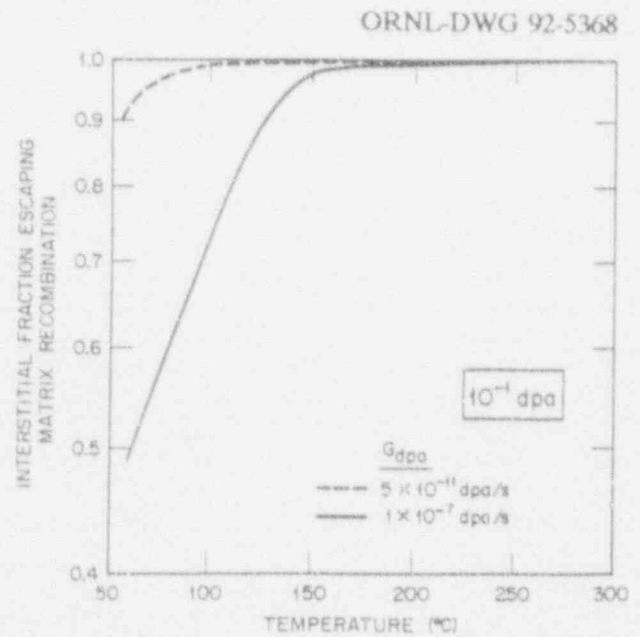
Figure 14. Influence of irradiation temperature on the fraction of interstitials lost to matrix recombination at a total dose of 0.1 dpa for displacement rates of 5×10^{-11} and 1×10^{-7} dpa/s.
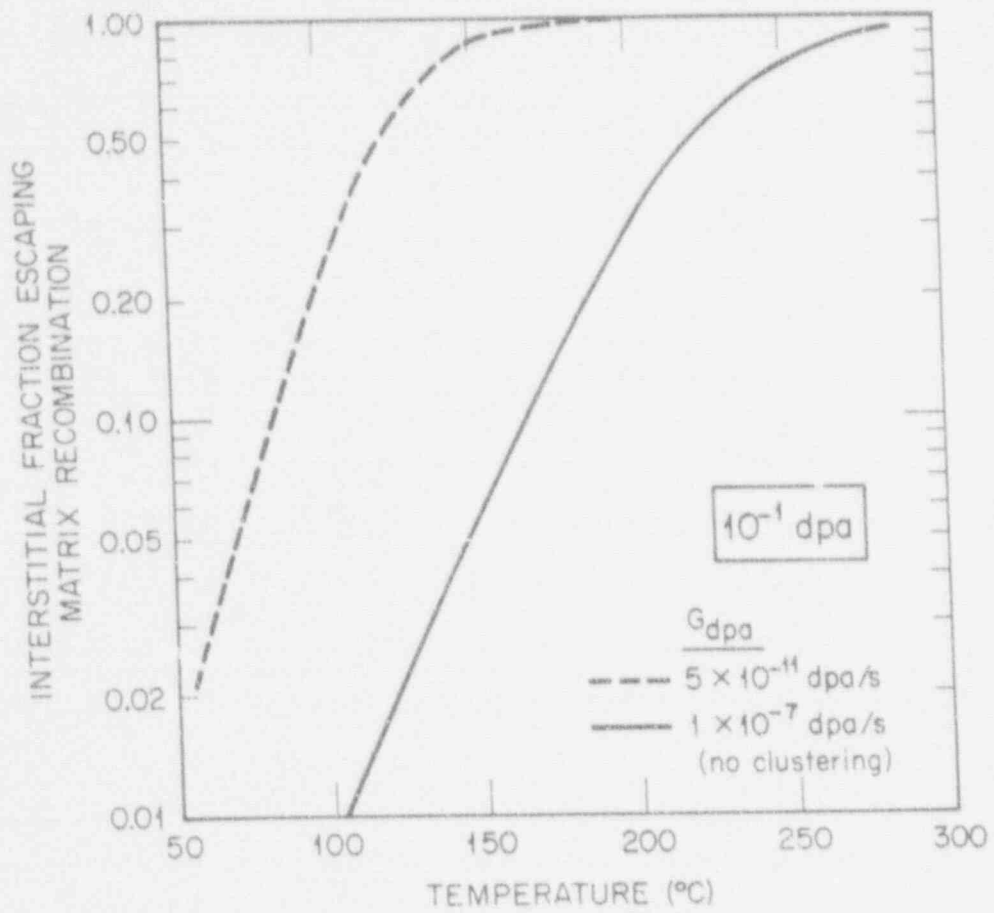
Figure 15. Influence of irradiation temperature on the fraction of interstitials lost to matrix recombination without point defect clustering, same conditions as Figure 14.

potential degree of strengthening that these defect clusters could cause.

The temperature dependence of the calculated strengthening due to interstitial and vacancy clusters at a dose of 0.1 dpa is shown in Figure 16. Results are included for both a low and a high displacement rate. The higher point defect supersaturations that are obtained at lower temperatures lead to much higher cluster densities and in turn greater strengthening. More strengthening is predicted at the higher displacement rate for the same reason. The strengthening tends to saturate below 100°C and has a fairly steep temperature dependence at higher temperatures. Vacancy clusters are responsible for more strengthening than are interstitial clusters at a given temperature and damage rate. This is a reflection of the higher value of β used for the interstitial clusters.

Similar trends are seen in Figure 17, where the predicted strengthening is shown as a function of displacement rate for irradiation temperatures of 60 and 285°C. At the lower temperature there is little dependence on the displacement rate since the defect cluster density has saturated. Vacancy clusters exhibit the greatest dependence on displacement rate at 285°C, but there is little influence of interstitial clusters at this temperature where the nucleation of small interstitial clusters is reduced.

The predicted strengthening shown in Figures 16 and 17 appears to be somewhat higher than what is experimentally observed, particularly at the lowest temperatures and highest damage rates. Reported values of irradiation-induced changes in the yield strength of RPV steels at 50 to 300°C are in the range of 35 to 350 MPa (5 to 50 ksi) (Cheverton et al., 1988; Lucas et al., 1987; Nanstad et al., 1988; and Odette and Lucas, 1989). In addition, a substantial component of the reported strengthening is believed to be due to copper-rich precipitates (Lucas et al., 1985; Odette, 1983; and Odette and Sheeks, 1981) which are not accounted for here. The use of one of the alternate barrier models discussed above would lead to lower calculated strengthening values. Reference to Figures 1 and 2 shows that the use of the softest barrier models (i.e., those based on Friedel's effective barrier spacing) would lead to

negligible strengthening for the conditions shown in Figures 16 and 17.

However, the dose of 0.1 dpa used in Figures 16 and 17 is higher than most RPV irradiation data and this could be responsible for some of the apparent discrepancy. The dose dependence of the predicted strengthening is shown in Figure 18, along with typical test reactor data and data from the HFIR surveillance program. The A533B data shown in Figure 18(a) are for the HSST plate-02 (Stallman, 1988) and the A302 data is the A302 correlation monitor (Stallman, 1988). Both materials were irradiated in the University of Virginia reactor in an experiment conducted by researchers from the University of California at Santa Barbara (Odette and Lucas, 1989). The HFIR data includes archive materials which were irradiated in the ORR (Cheverton et al., 1988). Reasonable agreement is observed between the calculations and the experimental data for the doses and displacement rates at which there are data. Some reduction in the barrier strength may be appropriate, particularly for the microvoids, but there does not appear to be a rationale for invoking one of the very soft barrier models.

Some interesting differences are observed between the behavior of the two cluster types at 285°C in Figure 18(a). The interstitial cluster contribution increases at a rate that is proportional to the square root of the dose until it saturates. The dose at which the yield strength change saturates is independent of the displacement rate, but the saturation level is proportional to the square root of the displacement rate. The strengthening due to vacancy clusters is also initially proportional to the square root of the dose, but the dose at which saturation occurs is a function of the displacement rate. At 60°C, Figure 18(b) indicates that saturation has not yet occurred at a dose of 0.1 dpa. This is related to the low defect mobility that leads to the long times required for the point defect concentrations to reach steady state as shown in Figure 6. There is little displacement rate dependence observed. Strengthening due to vacancy clusters exhibits the square-root dose dependence, but the dose dependence of the interstitial clusters is initially higher. The interstitial cluster strengthening has a dose dependence of about 0.75 at the lowest doses in

Figure 16. Temperature dependence of the calculated strengthening due to interstitial and vacancy clusters at 0.1 dpa for displacement rates of 5 x 10⁻¹¹ and 1 x 10⁻⁷ dpa/s.
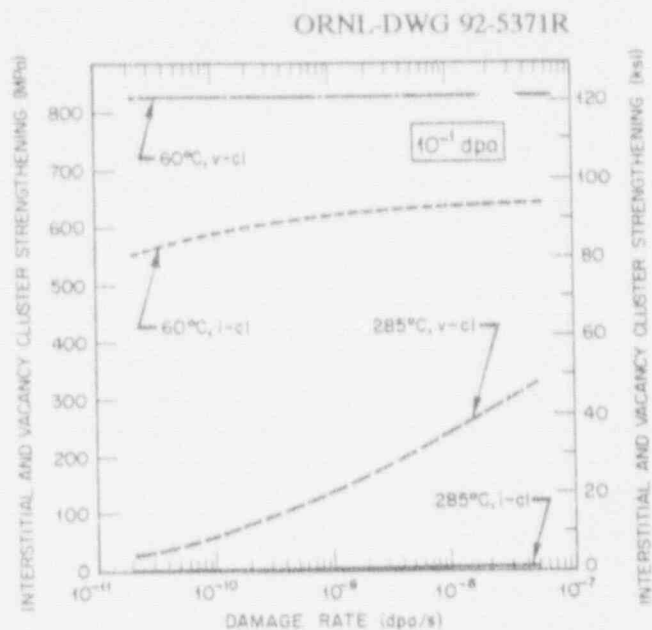
Figure 17. Displacement rate dependence of the calculated strengthening due to interstitial and vacancy clusters at 0.1 dpa for irradiation temperatures of 60 and 285° C.

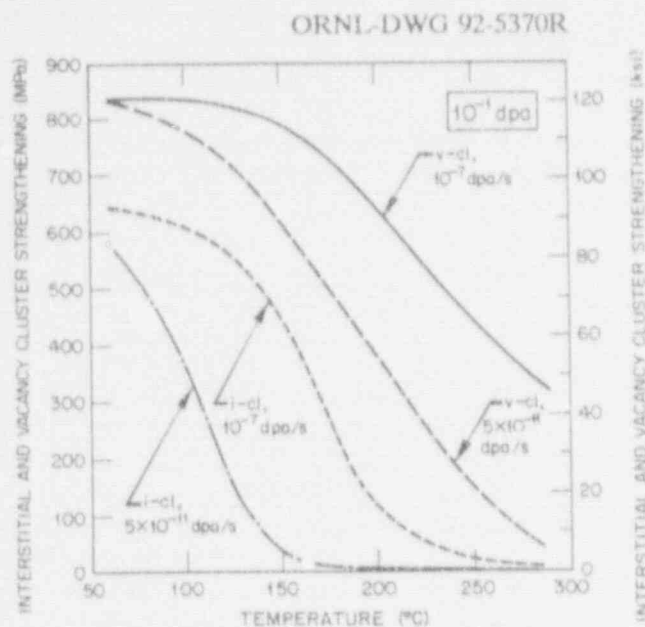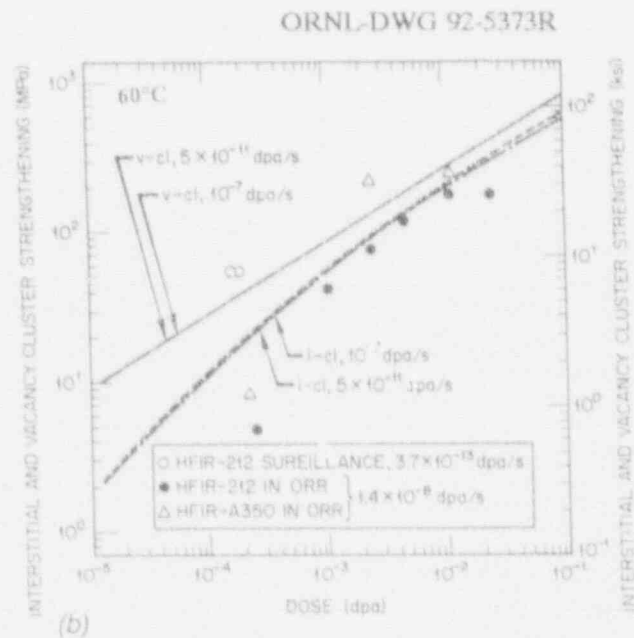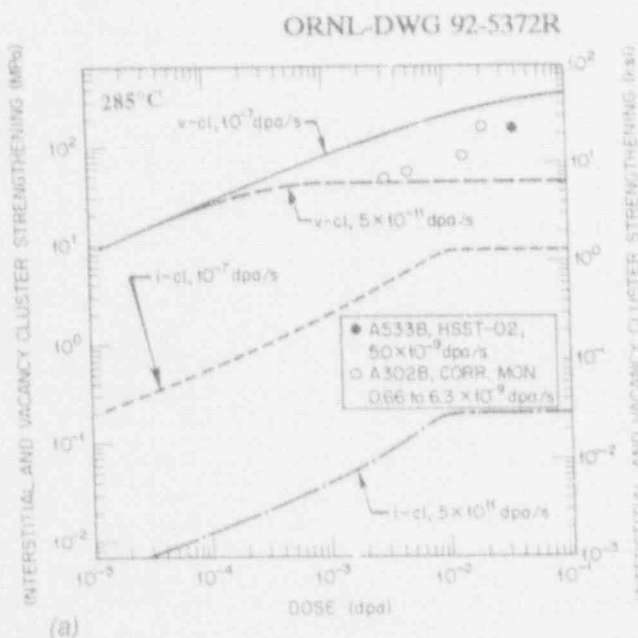Figure 18. Comparison of dose dependence of the calculated strengthening due to interstitial and vacancy clusters for displacement rates of 5 x 10⁻¹¹ and 1 x 10⁻⁷ dpa/s at 285° C (a) and 60° C (b) and typical data (Data from Cheverton et al., 1988 and Odette and Lucas, 1989).

Figure 18(b) and then undergoes a transition to square-root dependence. The interstitial cluster strengthening curves appear to be diverging at above 0.01 dpa and the behavior is likely to be similar to that shown in Figure 18(a) for 285°C if the calculations were carried out to much higher doses.

In order to better show the relative importance of the two types of defect clusters, the ratio of interstitial cluster strengthening to vacancy cluster strengthening is shown as a function of irradiation temperature and displacement rate in Figures 19 and 20. Vacancy clusters are clearly more important at higher temperatures and lower displacement rates. However, both types of clusters can produce a significant amount of strengthening. As mentioned above, there is probably some justification for reducing the barrier strength term for the vacancy clusters. For example, if a value of $\beta = 2$ was used for the vacancy clusters, the strengthening increment from the interstitial clusters would be comparable to or greater than that of the vacancy clusters for essentially all the conditions examined here. Thus, it seems appropriate to investigate the behavior of both cluster types in greater detail. Since the two defects will almost certainly behave differently under thermal annealing, this investigation may be necessary to understand the postirradiation annealing behavior and re-irradiation embrittlement of ferritic steels (Mader et al., 1992).

Summary and Planned Future Work

The motivation for this work is the need to develop an understanding of the physical mechanisms that lead to embrittlement in the ferritic steels used in LWRs. Such understanding is important to ensure the continued safe operation of these plants throughout their current license periods, and will become critical to plant life extension by license renewal. The calculations are intended to complement and aid in the analysis of the irradiation experiments that are conducted to investigate these same mechanisms. The work has focused on the displacement rate and irradiation temperature because these are key variables in data correlation and extrapolation. The displacement rate is important because many experiments are conducted at accelerated displacement rates in test reactors in order to obtain high fluence data in a reasonable time. The importance of irradiation temperature has

been highlighted recently by the HFIR surveillance data and is a concern for LWR support structures. This latter data have also raised concerns about displacement rate effects at very low displacement rates (Cheverton et al., 1989).

In order to investigate the range of irradiation temperatures of interest to LWR components, the time-dependent rate theory was used to develop a comprehensive model describing the evolution of point defects and point defect clustering. The time or dose required for the point defect concentrations to reach their steady state value is strongly dependent on the irradiation temperature and the sink structure that evolves under irradiation. For reasonable values of the microstructural parameters, for example, the time required for the point defects and the cluster populations to reach steady state can be very long at low temperatures. It is on the order of 30 years at 60°C. In addition, it was shown that the effect of displacement rate is different in the transient and steady state regimes. Thus, it appears that it is not appropriate to invoke the commonly used assumption of steady state defect concentrations when modeling low-temperature embrittlement or when analyzing the results of low-temperature experiments (Stoller and Mansur, 1990). The number or fraction of point defects that escape matrix recombination was used as a figure of merit to track the influence of the point defect transient.

The duration of the point defect transient may not be significant at the highest RPV operating temperatures, but these calculations clearly show that the transient needs to be considered at lower temperatures. However, some caution may be required in the use and interpretation of experiments conducted in test reactors, even at temperatures approaching 288°C. Test reactors typically have duty cycles in which the reactor operates for only several hours to a few days between shutdowns. Because of these frequent start-ups, experiments may be conducted mostly or entirely within the point defect transient, even at temperatures where the in-service component operates long enough for the point defects to be at steady state for most of its lifetime. Temperature and flux transients associated with reactor start-up have been shown to influence the the microstructure that evolves in elevated temperature irradiation (Kiritani et al., 1990). For components such as the HFIR, pressure vessel or LWR support structures that operate at temperatures below 100°C,

ORNL-DWG 92-5374R
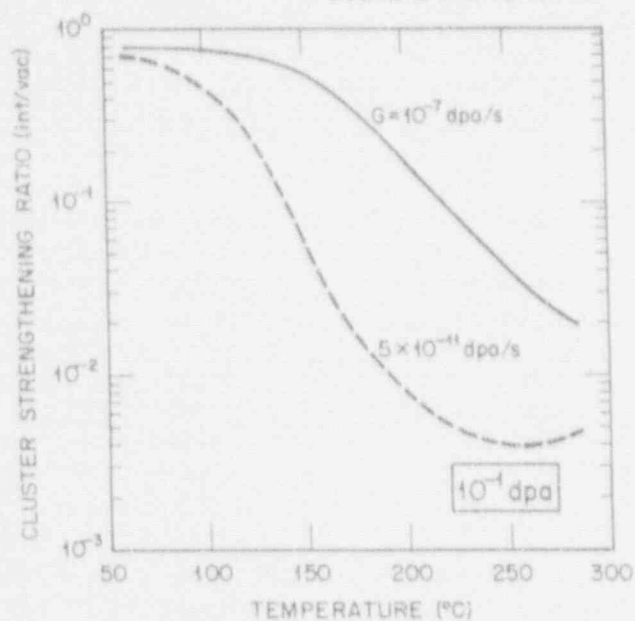
Figure 19.   Temperature dependence of the ratio
              of interstitial cluster to vacancy
              cluster strengthening at 0.1 dpa for
              displacement rates of 5×10^{-11} and
              1×10^{-7} dpa/s.

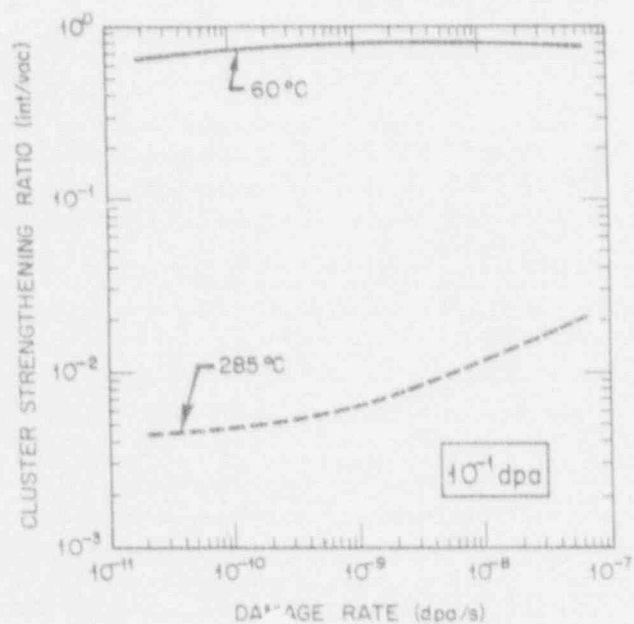ORNL-DWG 92-5375R

Figure 20.   Displacement rate dependence of the
              ratio of interstitial cluster to vacancy
              cluster strengthening at 0.1 dpa for
              irradiation temperatures of 60 and
              285° C.

the point defect transient may exceed the operating lifetime. These components and experiments operating in this temperature range can not be analyzed on the basis of the steady state theory.

The time-dependent model has been used to investigate the potential contribution of interstitial and vacancy clusters to radiation-induced strengthening in ferritic steels. Although there is some uncertainty in determining the strength of these clusters as barriers to dislocation motion, the results indicate that both cluster types could induce similar levels of strengthening. Using only the simplest barrier model, the calculated strengthening is comparable to that observed experimentally. Since this work has not included any strengthening contribution from radiation-induced precipitates, it appears that the cluster contribution obtained from the model is probably somewhat too large. However, it seems reasonable to conclude that these clusters play an important role in strengthening and that they may be responsible for greater strengthening than the copper-rich precipitates for some conditions of dose, displacement rate, and temperature. An understanding of their behavior under thermal annealing may be particularly important for interpreting postirradiation annealing studies and for predicting embrittlement under subsequent re-irradiation.

While many of the trends shown in Figures 16 through 20 can be understood in terms of the various reactions between the point defect and the cluster populations, some of the details are not yet fully understood. Further work is underway to develop an explanation for all the observed dependencies on displacement rate and dose, and to investigate the sensitivity of the model to variations in critical material parameters. Both the interstitial and interstitial clustering models require some further development to ensure that they are numerically well behaved for all the temperature and irradiation conditions of potential interest. The choice of the barrier strength terms used in Equations (20) and (21) need additional attention because of their key role in converting defect cluster densities to hardening. The range of uncertainty in these terms must be reduced to permit a determination of the relative importance of defect clusters and precipitates in irradiation hardening. Since the computing times required for the current model are

already rather long, some attention must be given to improving the efficiency of the calculations as more detail is incorporated. Finally, a version of the computer code will be developed to simulate interrupted irradiations and thermal annealing because of some of the concerns that were discussed earlier.

References

J. R. Beeler, Jr. and R. A. Johnson, Phys. Rev. **156**, 677-84, (1967).

A. L. Bement, Jr., "Fundamental Materials Problems in Nuclear Reactors," pp. 693-728 in *Strength of Metals and Alloys, Proceedings of Second International Conference*, Am. Soc. Met., Metals Park, Ohio (1970).

A. D. Brailsford and R. Bullough, Philos. Trans. R. Soc. **302**, 87-137 (1981).

R. D. Cheverton, J. G. Merkle, and R. K. Nanstad, Martin Marietta Energy Systems, Inc., Oak Ridge Natl. Lab., Oak Ridge, Tenn., *Evaluation of HFIR Pressure Vessel Integrity Considering Radiation Embrittlement*, ORNL/TM-10444, (1988).

R. D. Cheverton, F. B. Kam, R. K. Nanstad, and G. C. Robinson, Nucl. Eng. Des. **117**, 349-55 (1989).

G. E. Dieter, *Mechanical Metallurgy*, McGraw-Hill, New York (1976).

S. G. Druce, "Application of a United Kingdom Magnox Steel Irradiation Model to the HFIR Pressure Vessel," pp. 30-44 in *Effects of Radiation on Materials*, ed. N. H. Packan, R. E. Stoller, and A. S. Kumar, Am. Soc. Test. Mater., ASTM STP 1046, Vol. II, Philadelphia (1990).

C. A. English, W. J. Phythian, and A. J. E. Foreman, J. Nucl. Mater. **174**, 135-40 (1990).

C. A. English, A. J. E. Foreman, W. J. Phythian, D. J. Bacon, and M. L. Jenkins, "Displacement Cascades in Metals," p. 1 in *International Conference on Physics of Irradiation Effects in Metals, May 20-24, 1991, Siofok, Hungary*, Mater. Sci. Forum, Vol. 97-99 (1992).

M. L. Grossbeck, L. K. Mansur, and M. P. Tanaka, "Irradiation Creep in Austenitic Stainless Steels at 60 to 400°C with a Fusion Reactor Helium to dpa Ration," pp. 537-50 in *Effects of Radiation on Materials*, ed. N. H. Packan, R. E. Stoller, and A. S. Kumar, ASTM STP 1046, Vol. II, Am. Soc. Test. Mater., Philadelphia (1990).

G. Hettich, H. Mehrer, and K. Maier, Scr. Metall. **11**, 795-802 (1977).

K. W. Ingle, R. C. Perrin, and H. R. Schober, J. Phys. F., Met. Phys. **11**, 1161-73 (1981).

R. A. Johnson, J. Nucl. Mater. **83**, 147-59 (1979).

M. Kiritani, T. Yoskiie, S. Kojima, Y. Satoh, and K. Hamada, J. Nucl. Mater. **174**, 327-51 (1990).

T. Leffers and B. N. Singh, Radiat. Eff. **59**, 83-9 (1981).

G. E. Lucas, G. R. Odette, P. M. Lombrozo, and J. W. Sheckherd, "Effects of Composition, Microstructure, and Temperature on Irradiation Hardening of Pressure Vessel Steels," pp. 900-30 in *Effects of Radiation on Materials*, ed. F. A. Garner and J. S. Perrin, ASTM STP 870, Am. Soc. Test. Mater., Philadelphia (1985).

G. E. Lucas, G. R. Odette, R. N. Maiti, and J. W. Sheckherd, "Tensile Properties of Irradiated Pressure Vessel Steels," pp. 379-94 in *Effects of Radiation on Materials, Part 2*, ed. F. A. Garner, C. H. Henager, and N. Igata, ASTM STP 956, Am. Soc. Test. Mater., Philadelphia (1987).

E. Mader, G. E. Lucas, and G. R. Odette, "The Effects of Metallurgical and Irradiation Variables on the Post-Irradiation Annealing Kinetics of Pressure Vessel Steels," pp. 151-71 in *Effects of Radiation on Materials*, ed. R. E. Stoller, A. S. Kumar, and D. S. Gelles, ASTM STP 1125, Am. Soc. Test. Mater., Philadelphia (1992).

L. K. Mansur, Nucl. Tech. **40**, 5-34 (1978).

L. K. Mansur, Philos. Mag. A **39**, 497-506 (1979).

L. E. Murr, *Interfacial Phenomena in Metals and Alloys*, Addison-Wesley, Reading, Mass. (1975).

R. K. Nanstad, K. Farrell, D. N. Braski, and W. R. Corwin, J. Nucl. Mater. **158**, 1-6 (1988).

G. F. Odette, Scr. Metall. **17**, 1183-8 (1983).

G. R. Odette and G. E. Lucas, *Irradiation Embrittlement of LWR Pressure Vessel Steels*, EPRI NP-6114, Electric Power Research Institute, Palo Alto, Calif. (1989).

G. R. Odette and C. K. Sheeks, "A Model for Displacement Cascade Induced Microvoid and Precipitate Formation in Dilute Iron-Copper Alloys," pp. 415-36 in *Phase Stability During Irradiation*, ed. J. R. Holland, L. K. Mansur, and D. I. Potter, The Metallurgical Society of the AIME, Warrendale, Pa. (1981).

T. Diaz de la Rubia and M. W. Guinan, J. Nucl. Mater. **174**, 151-7 (1990).

T. Diaz de la Rubia and M. W. Guinan, "Mechanisms of Defect Production and Atomic Mixing in High Energy Displacement Cascades: A Molecular Dynamics Study," p. 1 in *International Conference on Physics of Irradiation Effects in Metals, May 20-24, 1991, Siofok, Hungary*, Mater. Sci. Forum, Vol. 97-99 (1992).

H. E. Schaefer, K. Maier, M. Weller, D. Herlach, H. Seeger, and J. Diehl, Scr. Metall. **11**, 803-9 (1977).

J. V. Sharp and A. J. E. Foreman, *Calculation of Build-up Times for Radiation Enhanced Diffusion*, AERE-R5786, U.K.A.E.A., Harwell Laboratory, Harwell, United Kingdom (1968).

F. W. Stallman, Martin Marietta Energy Systems, Inc., Oak Ridge Natl. Lab., Oak Ridge, Tenn., *Analysis of the A302B and A533B Standard Reference Materials in Surveillance Capsules of Commercial Power Reactors*, USNRC Report NUREG/CR-4947 (ORNL/TM-10459), (1988).

R. E. Stoller, M. L. Grossbeck, and L. K. Mansur, "A Theoretical Model of Accelerated Irradiation Creep at Low Temperatures By Transient Interstitial Absorption," pp. 517-29 in *Effects of Radiation on Materials: 15th Congerence*, ed. R. E. Stoller, A. S. Kumar, and D. S. Gelles, ASTM STP 1125, Am. Soc. Test. Mater., Philadelphia (1992).

R. E. Stoller and L. K. Mansur, "The Influence of Displacement Rate on Damage Accumulation in Irradiated Materials," pp. 52-67 in *Radiation Materials Science: Proceedings of the International Conference*, Ukrainian Academy of Sciences, Kharkov, USSR (1990).

R. E. Stoller and G. R. Odette, "The Effect of Helium of Swelling Influence of Cavity Density and Morphology," pp. 275-94 in *Effects of Radiation on Materials: 11th International Symposium*, ed. H. R. Brager and J. S. Perrin, ASTM STP 782, Am. Soc. Test. Mater., Philadelphia (1982).

R. E. Stoller and G. R. Odette, "A Comparison of the Relative Importance of Helium and Vacancy Accumulation in Void Nucleation," pp. 358-70 in *Radiation-Induced Changes in Microstructure: 13th International Symposium*, ed. F. A. Garner, N. H. Packan, and A. S. Kumar, ASTM STP 955, Am. Soc. Test. Mater., Philadelphia (1987).

R. E. Stoller and G. R. Odette, "A Composite Model of Microstructural Evolution in Austenitic Stainless Steel Under Fast Neutron Irradiation," pp. 371-92 in *Radiation-Induced Changes in Microstructure: 13th International Symposium*, ed. F. A. Garner, N. H. Packan, and A. S. Kumar, ASTM STP 955, Am. Soc. Test. Mater., Philadelphia (1987).

J. C. Van Duysen, J. Bourgoin, C. Janot, and J. M. Penisson, "Evolution of the Microstructure of PWR Pressure Vessel Steels from the CHOOZ A Reactor Surveillance Programme After Long Term Irradiations," pp. 117-30 in *Effects of Radiation on Materials: 15th Conference*, ed. R. E. Stoller, A. S. Kumar, and D. S. Gelles, ASTM STP 1125, Am. Soc. Test. Mater., Philadelphia (1992).

R. W. Weeks, S. R. Pati, M. A. Ashby, and P. Barranú, Acta Metall. 17, 1403-10 (1969).

W. G. Wolfer and M. Ashkin, J. Appl. Phys. 46, 547-57 (1975); and erratum in J. Appl. Phys. 46, 4108 (1975).

W. G. Wolfer, L. K. Mansur, and J. A. Sprage, "Theory of Swelling and Irradiation Creep," pp. 841-64 in *Radiation Effects in Breeder Reactor Structural Materials*, ed. M. L. Bleiberg and J. W. Bennet, AIME, New York (1977).

INTERNAL DISTRIBUTION

1.	D. J. Alexander	25.	R. K. Nanstad
2.	C. A. Baldwin	26.	W. E. Pennell
3.	E. E. Bloom	27.	C. E. Pugh
4.	R. D. Cheverton	28.	G. M. Slaughter
5-9.	W. R. Corwin	29.	S. Spooner
10.	D. F. Craig	30.	F. W. Stallman
11.	K. Farrell	31-40.	R. E. Stoller
12.	F. M. Haggag	41.	J. A. Wang
13.	S. K. Iskander	42-44.	M&C Records Office
14.	F. B. Kam	45.	ORNL Patent Office
15-21.	L. K. Mansur	46.	Central Research Library
22.	D. E. McCabe	47.	Document Reference Section
23.	J. G. Merkle	48-49.	Laboratory Records Department
24.	M. K. Miller	50.	Laboratory Records (RC)

EXTERNAL DISTRIBUTION

51-53. AEA TECHNOLOGY-HARWELL, Thermal Reactor Services, Oxfordshire
OX11 ORA Great Britain

    S. G. Druce
    C. A. English
    W. J. Phythian

54. ARGONNE NATIONAL LABORATORY, Material Science and Technology Division,
9700 South Cass Avenue, Argonne, IL 60439

    H. Weidersich

55. ATI, INC., Suite 160, 2010 Crow Canyon Place, San Ramon, CA 94583

    W. L. Server

56. BABCOCK AND WILCOX, 3315 Old Forest Road, Lynchburg, VA 24501

    A. ve

57-59. BATTELLE PACIFIC NORTHWEST LABORATORY, P-8-15, P.O. Box 999, Richland, WA 99352

      F. A. Garner
      H. Heinisch
      M. L. Hamilton

60-61. CEGB (Nuclear Electric), Berkeley Nuclear Labs., Berkeley, Gloucestershire GL 139 PB, United Kingdom

      J. Buswell
      R. B. Jones

62. CEN/SCK, Belgium, Reactor Physics Department, Boeretang 200, B-2400MOL, Belgium

      A. Fabry

63. ELECTRIC POWER RESEARCH INSTITUTE, P.O. Box 10412, Palo Alto, CA 94303

      T. Griesbach

64. GKSS RESEARCH CENTER, Max-Planck Strasse, Postfach 1160, D-2054 Geesthacht, GERMANY

      R. Kampmann

65. Sam P. Grant, 5313 Dixon Drive, Raleigh, NC 27609

66. LABORATOIRE DES SOLIDES IRRADIES', Ecole Polytechnique, 91128 Palaiseau Cedex, FRANCE

      A. Barbu

67. MATERIALS ENGINEERING ASSOCIATES, 9700B Martin Luther King, Jr. Highway, Lanham, MD 20706

      J. R. Hawthorne

68. NORTH CAROLINA STATE UNIVERSITY, Department of Nuclear Engineering, College of Engineering, Box 7909, Raleigh, NC 27695-7909

      K. L. Murty

69-73. NRC, RES/Division of Engineering, Washington, DC 20555

      A. Hiser
      M. E. Mayfield
      C. Z. Serpan
      L. C. Shao
      A. Taboada

74-75. NRC, Division of Engineering Technology, Washington, DC 20555

       B. J. Elliot
       K. R. Wichman

76-77. NRC, RES/Division of Safety Issue Resolution, Washington, DC 20555

       C. A. Hrabel
       R. E. Johnson

78. NRC, Region I, 631 Park Avenue, King of Prussia, PA 19406

       J. R. Strosnider

79. NUCLEAR INSTALLATIONS INSPECTORATE, Health and Safety Executive, St. Peter's House, Balliol Road, Bootle L203LZ, UNITED KINGDOM

       F. M. D. Boydon

80. OHIO STATE UNIVERSITY, Department of Metallurgical Engineering, Columbus, OH 43210-1179

       P. G. Shewman

81. PAUL SCHERRER INSTITUTE, CH-5233 Villigen PSI, SWITZERLAND

       G. Solt

82. ROLLS-ROYCE AND ASSOCIATES LTD., P.O. Box 31, Raynesway, Derby, England

       T. Williams

83. SANDIA NATIONAL LABORATORIES, Division 6471, Albuquerque, NM 87185-5800

       S. T. Rosinski

84. STAATL. MATERIALPRUFUNGSANSTALT, Pfaffenwalding 32, 7000 Stuttgart 80, Federal Republic of Germany

       J. Fohl

85. L. E. Steele, 7624 Highland St., Springfield, VA 22150-3931

86. TECHNICAL RESEARCH CENTRE OF FINLAND (VTT), Metals Laboratory, P.O. Box 26, SF-02151 Espoo, (Kemistintie 3, 02150 Espoo), FINLAND

       K. Torronen

87-88. UNIVERSITY OF CALIFORNIA, Department of Chemical and Nuclear Engineering, Ward Memorial Drive, Santa Barbara, CA 93106

       G. E. Lucas
       G. R. Odette

89. UNIVERSITY OF TOKYO, Department of Materials Science and Technology, 2641 Yamazaki Noda City, 278 JAPAN

       Professor Eng. N. Igata

90. UNIVERSITY OF TOKYO, Nuclear Fuels and Materials, Department of Nuclear Engineering, Faculty of Engineering, 7-3-1 Hongo, Bunkyo-Ku, Tokyo 113, JAPAN

       Professor S. Ishino

91-92. WESTINGHOUSE ELECTRIC CORPORATION, P.O. Box 355, Pittsburgh, PA 15230

       T. Mager
       R. C. Shogan

93-94. WESTINGHOUSE SCIENCE AND TECHNOLOGY CENTER, 1310 Beulah Rd., Pittsburgh, PA 15235

       M. G. Burke
       R. G. Lott

95. DOE, Division of Materials Sciences, ER-131, MS GS-236/GTN, Washington, DC 20585

       J. B. Darby

96. DOE OAK RIDGE FIELD OFFICE, P.O. Box 2008, Oak Ridge, TN 37831-6269

       Office of Deputy Assistant Manager for Energy Research and Development

97-98. DOE, OFFICE OF SCIENTIFIC AND TECHNICAL INFORMATION, P.O. Box 62, Oak Ridge, TN 37831

99-160. Given distribution as shown in category RF (NTIS-10)

U.S. NUCLEAR REGULATORY COMMISSION

BIBLIOGRAPHIC DATA SHEET

(See instructions on the reverse)

2. TITLE AND SUBTITLE

Modeling the Influence of Irradiation Temperature and
Displacement Rate on Radiation-Induced Hardening in
Ferritic Steels

3. DATE REPORT PUBLISHED	
MONTH	YEAR
July	1992

4. FIN OR GRANT NUMBER
L1098

5. AUTHOR(S)

R. E. Stoller

6. TYPE OF REPORT

Technical

7. PERIOD COVERED *(Inclusive Dates)*

8. PERFORMING ORGANIZATION — NAME AND ADDRESS *(If NRC, provide Division, Office or Region, U.S. Nuclear Regulatory Commission, and mailing address; if contractor, provide name and mailing address.)*

Oak Ridge National Laboratory
Oak Ridge, TN 37831-6285

9. SPONSORING ORGANIZATION — NAME AND ADDRESS *(If NRC, type "Same as above"; if contractor, provide NRC Division, Office or Region, U.S. Nuclear Regulatory Commission, and mailing address.)*

Division of Engineering
Office of Nuclear Regulatory Research
U.S. Nuclear Regulatory Commission
Washington, DC 20555

10. SUPPLEMENTARY NOTES

11. ABSTRACT *(200 words or less)*

The influence of irradiation temperature and displacement rate have been investigated using a model based on the reaction rate theory description of radiation damage. This theory was developed primarily for the investigation of relatively high-temperature, high-dose radiation effects such as void swelling and irradiation creep. Before applying that theory to the much lower temperature and dose regimes characteristic of light water reactor pressure vessels and support structures, it is necessary to examine the assumptions made in formulating the theory. The major simplifying assumption that has commonly been made is that the interstitial and vacancy concentrations reach a quasi-steady state condition rapidly enough that the steady state concentrations can be used in calculating the observable radiation effects. The results presented here indicate that the assumption of steady state point defect concentrations is not valid for temperatures much below the light water reactor pressure vessel operating temperature of about 288°C. At lower temperatures, the time required for the point defect concentrations to reach steady state can exceed an operating reactor's lifetime. Even at 288°C, the point defect transient time can be long enough to influence the interpretation of irradiation experiments done in materials test reactors at accelerated damage rates.

Based on the insights obtained with the simple models of point defect evolution, a more detailed model was developed that incorporates an explicit description of point defect clustering. These clusters are potentially responsible for the fraction of the radiation-induced hardening that is attributed to the so-called "matrix defect." The model considers both interstitial and vacancy clustering. The former are treated as Frank loops while the later are treated as microvoids. The point defect clusters can be formed either directly in the displacement cascade or by diffusive encounters between free point defects. The results of molecular dynamics simulation studies are used to provide guidance for the clustering parameters. The hardening due to point defect clusters was calculated using a simple dislocation barrier model. The results indicate that both interstitial and vacancy clusters can give rise to significant hardening. The relative importance of each cluster type is shown to be a function of irradiation temperature and displacement rate.

12. KEY WORDS/DESCRIPTORS *(List words or phrases that will assist researchers in locating the report.)*

radiation effects	displacement rate
pressure vessel steels	point defect clusters
hardening	yield strength
embrittlement	radiation damage
theoretical models	ferritic steels
irradiation temperature	

13. AVAILABILITY STATEMENT

Unlimited

14. SECURITY CLASSIFICATION

(This Page)

Unclassified

(This Report)

Unclassified

15. NUMBER OF PAGES

16. PRICE

NUREG/CR-5859

MODELING THE INFLUENCE OF IRRADIATION TEMPERATURE AND DISPLACEMENT
RATE ON RADIATION-INDUCED HARDENING IN FERRITIC STEELS

JULY 1992

UNITED STATES
NUCLEAR REGULATORY COMMISSION
WASHINGTON, D.C. 20555-0001

OFFICIAL BUSINESS
PENALTY FOR PRIVATE USE, $300